Technische Universität Braunschweig

Institut für Raumfahrtsysteme

J 2207 M

Development of an Optically Accessible Strand Burner for Green Monopropellant Combustion Rate Studies

Institute of Space Systems & DLR Institute of Space Propulsion

Joshua Haase

October 7, 2022

Technische Universität Braunschweig

Institute of Space Systems

Technische Universität Braunschweig | Institute of Space Systems
Hermann-Blenk-Str. 23 | 38108 Braunschweig | Germany

Technische Universität
Braunschweig
Institute of Space Systems

Head of Institute

Hermann-Blenk-Str. 23
38108 Braunschweig
Germany

Dr.-Ing.
Carsten Wiedemann

Tel. +49 (0) 531 391-9970
Fax +49 (0) 531 391-9966
c.wiedemann@tu-braunschweig.de
www.space-systems.eu

Date: 15. Februar 2022

Your abbreviation:
Date of your message:
Our abbreviation: CW
Date of our message:

Master thesis
of Mr. cand. mach. Joshua Haase
Matr.-No. 4974877

Subject:
Development of an optically accessible Liquid Propellant Strand Burner for Green Monopropellant Combustion Rate studies
(Entwicklung eines optisch zugänglichen Flüssigtreibstoff-Strand-Burners zur Untersuchung der Abbrandrate von Green Monopropellants)

Gelled monopropellants, oxidizers and fuels potentially offer significant benefits compared to conventional solid, liquid or hybrid propellants. Therefore, in Germany a development program on that topic was started in the early 2000s. The motivation for this is unique features gelled propellants possess. One of the strongest assets is the altering of the rheological behavior: these thickened liquids with a distinct yield point behave like solids at rest. This improves handling and storage properties since the propellant neither can be accidently spilled nor it can leak out and form pools that potentially can be the source of fires. Additionally, altering rheological properties allow for incorporation of metal fuels, energetic materials and combustion and ignition catalysts. By this means energy density and combustion properties of gelled propellants can be enhanced and/or tailored.

In the last decade research at DLR Institute of Space Propulsion was focused on gelled nitromethane monopropellant rheology and combustion. Yet undisclosed test results show that monopropellant gel combustion is altered compared to neat nitromethane combustion. Especially the gelling agent and carbon particles admixtures seem to play a crucial role. In the last two years a new research stream gained momentum: in order to further enhance propellant performance and density new additives were introduced. Among them are carbon nanoparticles and organometallic complexes. In a recently completed Master's thesis the ignition and combustion behavior of neat nitromethane droplets and droplets of nitromethane mixtures containing Fe- & Cr-compounds, and carbon nanoparticles in different atmospheres at pressures of 1, 3, 5 and 8 bar was examined. Even though nitromethane is a known monopropellant ignition could only be achieved in atmospheres containing

oxygen. Under nitrogen even at 8 bar ignition could not be achieved: this was the case in both, neat and additive-containing droplets. A possible reason for this is the fact that nitromethane is difficult to ignite – Boyer (2006) was not able to ignite nitromethane even at pressures in the order of 200 bar in a nitrogen atmosphere. In previous work the experiments were constrained to liquid-like propellant mixtures – viscous specimens and gels could not be used since droplets could not be generated. Additionally, it is not clear if the measured droplet combustion rate was estimated correctly. This may be because the droplet moved on the holding rod and changed its shape during combustion.

In order to compare droplet regression rate with a more conventional means of combustion rate measurement, to address ignition issues and to enable measurements of viscous and gel-like specimens an experimental setup shall be implemented. Within this setup propellant shall be burned in a preferably transparent tube which is located in a pressure chamber able to create controlled initial atmospheric conditions with pressures of up to 80 bar. A means of ignition such as a pyrotechnic grain, a glow plug or a torch shall be provided. With this setup the effect of various propellant additives on the combustion behavior on nitromethane shall be evaluated under high pressures.

Phase 0: Preliminary Design

- Literature research
- Preliminary tests
- Requirement & constraint definition (especially concerning test safety)

Phase 1: Test Chamber Design and Development

- Design of a test chamber with optical access capable of combustion for several seconds at pressures of up to 80 bar.
- Design of a means to remove combustion gasses from the chamber to prevent overpressure
- Design of a liquid propellant column holder (glass tube or alike)
- Design and characterization of a means of ignition with a variable and well-defined ignition temperature and/or energy
- Design of a means to evaluate combustion rate history such as a high-speed video evaluation setup coupled with a Python-based image analysis tool.
- Definition and installation of measurement hardware such as:
    - High speed video camera
    - Chamber pressure measurement and monitoring
    - Data acquisition system to synchronize and save pressure data (optional)

Phase 2: Run-In Test Campaign

Objective: Evaluate ignition time and combustion rate in nitrogen atmosphere at high pressure (approx. 20…50 bar) for pure nitromethane in order to find lower combustion pressure limit within the created test setup.

Phase 3: Additives test campaign (optional)

Objective: Evaluate the influence of additives on NM ignition and combustion behavior in nitrogen atmosphere at 20, 30, 40, 50 bar

Additives:

- 2 kinds of inhibitors in two loadings (n-Butanol, Nitroethane, Ethanol and the like)

- 2 ignition/combustion catalysts (Fe- & Cr-compounds and the like)
- 2 kinds of nanoparticles (CNT, graphene, graphene oxide)

Final propellant mixtures are tbd. Depending on time constraints parts or phase 3 entirely may be omitted.

At the beginning of the thesis a definition and description of individual work packages has to be carried out (Work Breakdown Structure, Work Package Description), which then have to be merged to a project schedule. The thesis has to be prepared according to the guidelines of the Institute of Space Systems and submitted bounded in one original version.

The Institute of Space Systems supports the scientific publication of their student's theses with prior permission; nevertheless disposing of the results is only allowed after consultation of the mentoring institutions. Passing on to a third party or publication of this thesis is only allowed after consultation of the mentoring institutions. The thesis remains property of the mentoring institutions.

Literature:

Boyer, 2005, Combustion characteristics and flame structure of nitromethane liquid monopropellant

Chang, 2002, Assessment of Combustion Characteristics and Mechanism of Hydroxylammonium Nitrate-Based Liquid Monopropellant

Derk, 2019, High Pressure Burning Rates of JA2 and Nitromethane Propellants

Fuller, 2020, A continuous flow liquid propellant strand burner for high pressure monopropellant and bipropellant combustion studies

Gudnason, 2010, Characterization of Potassium Nitrate - Sugar Alcohol Based Solid Rocket Propellants

Ide, 2015, Potential of ADN-based Ionic Liquid Propellant for Spacecraft Propulsion

Ide, 2016, Combustion Characteristics of an Ammonium-Dinitramide-Based Ionic Liquid Propellant

McCown, 2014, Experimental Techniques to Study Linear Burning Rates of Heterogeneous Liquid Monopropellants

Ziemer, 2021, Influence of Organometallic Complexes and Carbon Nanoparticles on Nitromethane Droplet Combustion

Timeframe: 6 months
Tutors: Dr.-Ing. Carsten Wiedemann, Declan Jonckers and project scientists
Maxim Kurilov (DLR)

Issued on:

Submitted on:

Dr.-Ing. Carsten Wiedemann

Eidesstattliche Erklärung

Ich erkläre hiermit an Eides Statt, dass ich die nachfolgende Arbeit selbständig und nur unter Zuhilfenahme der angegebenen Literatur angefertigt habe.

_____

Datum, Unterschrift

Abstract

In line with the current trends toward replacing hydrazine, the current state-of-the-art monopropellant for in-space propulsion applications, the German Aerospace Center (DLR) Institute for Space Propulsion has recently devoted considerable efforts into researching and developing novel, green alternatives. Nitromethane (NM) has been identified as one such alternative, showing great potential due its good performance characteristics, low toxicity and wide availability. In this thesis the effects of two catalyst additives, an iron-based organometallic compound (OMC1) and chromium(III) acetylacetonate (CAA) and of two inhibitor additives, a organosulfur compound (OSC1) and n-butanol (BUT), on the combustion rate of nitromethane were studied. For this purpose a liquid propellant strand burner was developed capable of igniting and burning monopropellants in inert atmospheres at pressures up to 6 MPa. In order to obtain combustion rates from high-speed-camera footage recorded during tests an image analysis tool was implemented in Python. Results showed that the addition of a catalyst significantly increased overall combustion rates when compared to neat NM, with a mixture containing 2 wt.% OMC1 producing the best results. Furthermore, it was observed that the addition of OMC1 led to a lowering of the minimum pressure at which sustained combustion could be achieved to 1.54 MPa from 3 MPa. Notably, for a mixture containing 2 wt.% OMC1 and 13 wt.% of the inhibitor additive OSC1, a further decrease of the minimum pressure to 1.24 MPa was observed, which coincides with pressure levels typical in monopropellant thrusters, making this a potentially viable alternative to hydrazine.

Übersicht

Als Folge des aktuellen Trends zum Ersatz von Hydrazin, dem derzeitigen Standard für monergole Satelliten- und Orbitalantriebe, hat das Institut für Raumfahrtantriebe des DLR in den letzten Jahren erhebliche Forschungsarbeit zur Entwicklung neuartiger, grüner Alternativen betrieben. Nitromethan NM wurde aufgrund guter Leistungsmerkmale, geringer Toxizität und einfacher Verfügbarkeit als Alternative mit hohem Potential identifiziert. In der vorliegenden Arbeit wurden die Wirkungen von zwei Additiven mit katalytischer Wirkung, der eisenbasierten Organometallischen Verbindung OMC1 und Chrom(III)-acetylacetonat (CAA), sowie von zwei Additiven mit inhibitiver Wirkung, der Organoschwefelverbidung OSC1 und n-Butanol BUT, auf die Abbrandrate von Nitromethan untersucht. Zu diesem Zweck wurde ein Flüssigtreibstoff-Strangbrenner entwickelt, der Monergole in inerten Atmosphären bei Drücken bis zu 6 MPa zünden und verbrennen kann. Um die Abbrandraten aus den während der Tests aufgezeichneten Hochgeschwindigkeitsaufnahmen zu bestimmen, wurde ein Bildanalyse-Tool in Python implementiert. Die Ergebnisse zeigten, dass die Zugabe eines Katalysators die Abbrandraten über den gesamten Druckbereich im Vergleich zu reinem NM deutlich erhöhte, wobei ein Gemisch mit 2 Gew.-% OMC1 die besten Ergebnisse lieferte. Darüber hinaus wurde beobachtet, dass die Zugabe von OMC1 zu einer Senkung des minimalen Drucks, bei dem eine anhaltende Verbrennung stattfindet, von 3 MPa auf 1.54 MPa führte. Weiterhin wurde bei einem Gemisch, das 2 Gew.-% OMC1 und 13 Gew.-% OSC1 enthielt, eine weitere Senkung des Drucks auf 1.24 MPa beobachtet. Dieser Druck ist mit den für monergole Satelliten- und Orbitalantriebe typische Brennkammerdrücken vergleichbar. Es konnte damit nachgewiesen werden, dass NM bei eine potenziell tragfähige Alternative für Hydrazin darstellt.

Contents

1 Introduction

Satellites and other spacecraft require rocket propulsion systems in order to maneuver in the vacuum of space. One widespread form of rocket propulsion for in-space propulsion applications are liquid bi- or monopropellant thrusters [1]. Figure 1.1 shows a famous example for one such system. It depicts the forward Reaction Control System (RCS) on the nose of the US Space Shuttle. The RCS consisted of multiple thrusters at various positions and orientations - visible as openings in the hull for the nozzles from which the exhaust gases are expelled - which allowed the Shuttle to adjust its attitude and perform orbital maneuvers. The system used in the Space

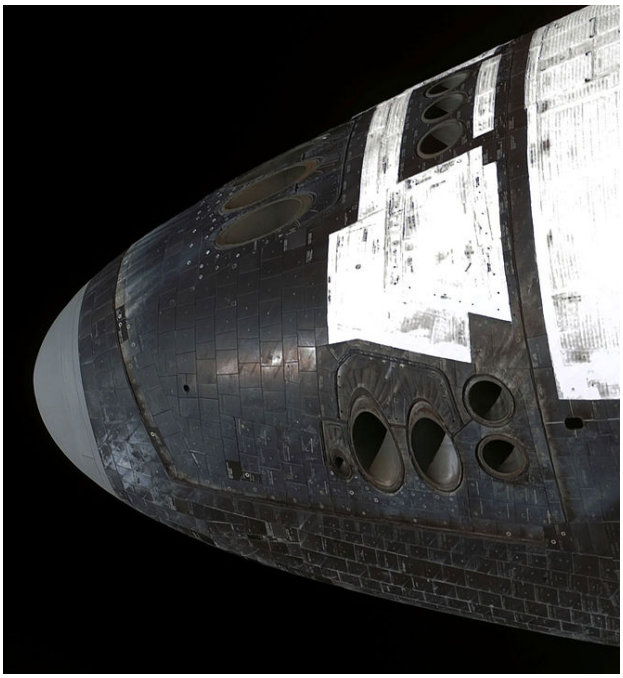

Figure 1.1: Space Shuttle forward Reaction Control System (RCS). Nozzle openings in the hull indicate the position and orientation of the thrusters. The system utilized a propellant combination of monomethylhydrazine (MMH) as fuel and nitrogen tetroxide (N_2O_4) as the oxidizer [1, 2].

Shuttle is a liquid bi-propellant system, meaning that the propellant consists of two components, fuel and oxidizer, both of which are present in a liquid state and are stored in separate tanks. Figure 1.2a shows such a system. While these systems provide the best properties in terms of performance and versatility, these benefits come at the cost of high complexity and cost [1]. Therefore, another common choice for spacecraft propulsion are monopropellant systems, shown in figure 1.2b. As the name suggests these systems operate with only a single propellant, greatly reducing the amount of components necessary leading to lower complexity and costs.

Historically the only monopropellants that meet these requirements, while also providing the necessary performance capabilities, are hydrazine (N_2H_4) and its derivatives monomethylhydrazine

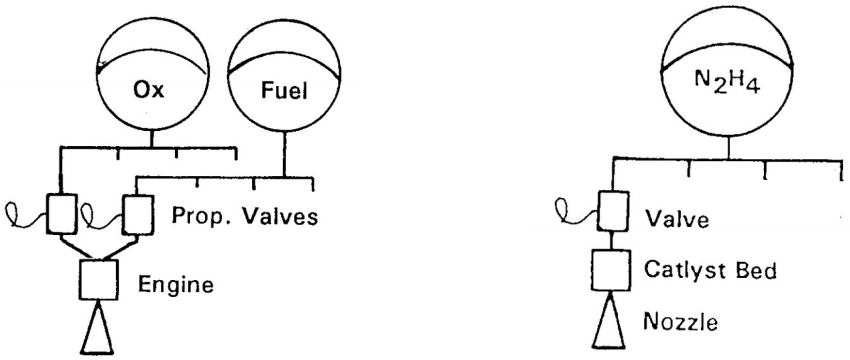

(a) Bi-propellant system.

(b) Monopropellant system.

Figure 1.2: Schematic diagrams of typical propulsion systems for in-space propulsion applications. [1]

(MMH) and unsymmetrical dimethylhydrazine (UDMH). Since the 1960s hydrazine has been used almost exclusively as a propellant for in-space propulsion applications. This is a result of its good performance and storage capabilities. Decomposition can be reliably achieved by use of the Shell 405 catalyst [3]. Additionally, seeing intense use over the decades, hydrazine technology has matured and has become the go-to choice even for modern space missions.

However, due to hydrazine's high toxicity and carcinogenicity many recent research efforts have been devoted to non-toxic 'green' alternatives [3]. This trend is further being driven by the European Commission's listing of hydrazine as a substance of very high concern and its decision to seek to greatly restrict or ban the use of hydrazine as part of its Registration, Evaluation, Authorization and Restriction of Chemicals (REACH) legislation [4, 5]. Due to the special equipment required for handling and the replacing of hardware damaged by corrosion, ground costs for hydrazine are increasing [4]. Figure 1.3 shows an image taken during the fueling operations of the recently launched James Webb Space Telescope. Personnel are required to wear the most severe Personal Protective Equipment (PPE) in the form of Self Contained Atmospheric Protection Ensemble (SCAPE) suits and work with the utmost caution while handling hydrazine [4]. This also influences other ground operations as it requires the evacuation of any personnel not necessary for the fueling process which leads to delays of ground operations [4]. All of these listed reasons have lead cost and handling of hydrazine to become increasingly problematic, outweighing the advantages in storage and performance capabilities.

In line with this trend the German Aerospace Center (DLR) Institute for Space Propulsion's department for Satellite- and Orbital Propulsion is investigating a variety of these 'green' propellants and other future fuels. To aid in this effort a method of characterizing propellants in an easily controlled environment and in a highly repeatable manner has been identified in the form of a strand burner. The goal of this thesis is to develop such a test stand and to demonstrate its use in a test campaign for nitromethane-based propellants.

Figure 1.3: James Webb Space Telescope during fueling operations prior to launch at Europe's Spaceport in French Guiana [6].

1.1 Scientific Goals

Research Motivations

Nitromethane (NM) as a monopropellant has been identified by numerous studies as a potential green alternative for hydrazine [4, 5, 7, 8]. It is non-toxic and non-carcinogenic according to the European Chemicals Agency [9]. Furthermore, as an industrial chemical with a variety of current applications other than propulsion it is widely available at relatively low cost [7, 10].
The main performance parameters by which monopropellants are typically characterized are specific impulse I_{sp}, volumetric impulse $I_{sp,vol}$ and combustion temperature. Figure 1.4 compares the performance characteristics of neat nitromethane to those of hydrazine and other state of the art (SOTA) green monopropellants based on the aforementioned parameters [10]. Nitromethane significantly outperforms hydrazine in both specific impulse and volumetric impulse. However, the good performance comes with the drawbacks of multiple issues that would require being addressed before nitromethane can be considered a suitable replacement for hydrazine. For one higher combustion temperatures, and consequently higher chamber temperatures, would necessitate the use of higher cost materials materials or engine level design solutions not required for hydrazine-based systems [5]. Nitromethane's slow combustion rate results in increased characteristic chamber lengths L^*, meaning larger, higher mass engines are necessary to achieve complete combustion [11, 12]. A number of studies reported difficulties initiating nitromethane combustion at lower pressures, achieving this only at pressure levels significantly higher than those common for monopropellant thrusters [8, 13, 14]. Higher pressures likewise lead to an increase in mass in comparison to hydrazine systems. Finally, while combustion may be hard to initiate, detonation

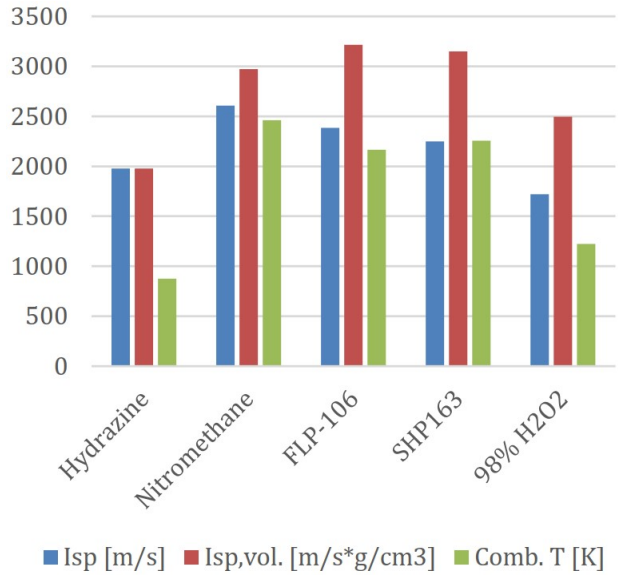

Figure 1.4: Performance parameters of green monopropellants and hydrazine. With I_{sp} as specific impulse, $I_{sp,vol}$ as volumetric impulse and combustion temperature [10].

can occur when supplied with sufficient energy from a shock [7, 10]. These characteristics lead to issues regarding handling and transportation of the proposed monopropellant.

All of the aforementioned issues may be addressed by the use of propellant additives. Additives offer the ability to tailor the combustion behavior in order to increase the range of nitromethane applications [15]. Various studies found that the addition of metals, metal oxides and silica [8, 15, 16, 17] had a catalytic effect and significantly increased combustion rates while increasing the specific impulse. Addition of nanoscale graphene sheets resulted in increased burn rates at lower combustion temperatures [18]. Finally, studies conducted in the past and more recently at the DLR found n-butanol to be an effective inhibitor reducing shock sensitivity to acceptable levels [7, 10, 19]. All of these approaches show great promise but further development is necessary until a nitromethane-based monopropellant system can be considered for in-space propulsion applications. In the previously mentioned studies combustion rates of neat nitromethane and nitromethane-based mixtures were determined at pressure levels above those common for monopropellant thrusters - as low as 1.0 MPa and not higher than 4.0 MPa [1] - usually due to the fact that combustion could not be initiated. Combustion rate studies at lower pressures are necessary to identify suitable additives that can enable combustion at these pressure levels and ideally lower the minimum pressures at which combustion can still be achieved. Furthermore, while separate issues were addressed in an isolated fashion, aiming only to increase performance or else improve handling characteristics, the effects of combining both catalytic and inhibiting additives in order to create a mixture that more closely meets the requirements of a rocket propellant have not yet been studied. Finally, while a great variety of promising additives have already been identified, having the ability to easily test and evaluate newly found or developed substances would greatly aid in the development of a suitable green alternative to hydrazine.

Research Objectives

The primary objective of this thesis is to develop an experimental setup with which combustion rate studies for green monopropellants can be carried out. The proper functioning of this test stand is to be proven during run-in test campaign with pure nitromethane at pressures around and below those typical for monopropellant thrusters. Following this the effect of various catalyst and inhibitor additives, both in isolation and combined, on the combustion behavior of nitromethane will be studied during the subsequent additives test campaign, in order to determine additives that would make nitromethane a feasible option for future green monopropellant in-space propulsion applications.

1.2 Method of Approach

Following this introduction the results of a literature research regarding similar experimental setups, the SOTA of monopropellants, green monopropellants, nitromethane and propellant additives will be presented in chapter 2. Chapter 3 will begin with a definition of the requirements. Following this a description of the design process is presented. The resulting final strand burner design will then be presented by means of 3D-models. Following this the remaining components including the data acquisition and control system will be presented. Chapter 5 will offer a description of the image analysis tool that was developed to measure combustion rates. In chapter 6 the results of both the run-in and additives test campaign will be presented and discussed. A conclusion will be drawn in chapter 7 summing up key findings followed by suggestions for future work in chapter 8.

2 Background

The following chapter presents a short introduction into rocket and space propulsion and includes relevant performance parameters used to asses rocket propellants. Next, it introduces an overview of current state of the art green monopropellants with a focus on nitromethane, the propellant that is studied within the present work. Finally, previous nitromethane combustion rate studies are discussed and the propellant additives selected to be studied in the course of this thesis are presented.

2.1 Rocket and Space Propulsion

Propulsion can be broadly described as "the act of changing the motion of a body" [11, p. 1]. This change is achieved by applying a force provided by a propulsion mechanism onto the body [11]. In the case of rocket propulsion this force, or thrust, is produced by ejecting matter at high velocity and thus imparting a reaction force onto the flying vehicle [11].

Rocket propulsion is singular compared to other forms of propulsion in the sense that it requires no outside medium as reaction mass for the propulsion system to act upon. Instead, it carries the reaction mass within the vehicle as propellant and additionally does not require a surrounding medium as the 'working fluid'. Therefore, in comparison to other forms of propulsion, rocket engines can operate in every environment, even the vacuum of space [11, 20].

2.1.1 Rocket Propulsion Principles

The underlying physical principle that governs the rocket propulsion mechanism is Newton's third law: the law of action and reaction. It states, that when two bodies A and B interact, the forces applied to one another are equal and opposite as described in equation 2.1 [20, 21].

$$F_{A \to B} = -F_{B \to A} \tag{2.1}$$

In the case of a spacecraft or rocket body A is the vehicle itself and B is the ejected matter (propellant) in the form of the exhaust gases. The thrust generated by the exhaust is a function of exhaust mass flow $\dot{m}$ and exit velocity v_e of the ejected matter as described in equation 2.2, Newtons second law [11, 21].

$$F = \dot{m} \cdot v_e \tag{2.2}$$

In 1903 Konstantin Tsiolkovsky published a paper in which he derived an equation for describing the motion of a rocket, a vehicle whose mass is continuously decreasing as it expels matter rearwards. By applying these dynamics to the aforementioned Newton's laws, Tsiolkovsky obtained a

formula for the change of velocity Δv of the vehicle while taking into account its changing mass. It is known as the rocket equation 2.3 [20, 21].

$$\Delta v = v_e \cdot \ln\left(\frac{m_0}{m}\right) \tag{2.3}$$

With m_0 as the starting mass of the rocket at ignition and m as mass of the rocket after propellant has been expelled. This equation identifies exit velocity as an important performance parameter for a rocket engine. However, it also signifies the importance of vehicle dry mass, that is vehicle mass without propellant, since a lower dry mass allows the loading of more propellant while maintaining the same starting mass m_0. This results in an increased mass ratio $\frac{m_0}{m}$ and thus in a greater increase in vehicle velocity.

2.1.2 Performance Parameters

While exhaust velocity and mass ratio are important performance parameters, further parameters can be useful to characterize a rocket propulsion systems performance. The most commonly used are total impulse I_t and specific impulse I_{sp}. Total impulse I_t is derived by integrating the thrust force from equation 2.2 over burning time. When assuming constant thrust and very short start and stop transients it can be described by equation 2.4 [11].

$$I_t = F \cdot t \tag{2.4}$$

The total impulse I_t is proportional to the total energy released by the stored propellant in a propulsion system [11]. While it is a good indicator for the performance of a given system, it depends on the propellant mass used to achieve the burning time used in the calculation. The specific impulse I_{sp} is a more suitable parameter when trying to compare different propulsion systems to one another as it eliminates the propellant mass from the calculation as shown in equation [11].

$$I_{sp} = \frac{I_t}{m_p \cdot g_0} \tag{2.5}$$

Here m_p is the propellant mass and g_0 is the standard acceleration of gravity at sea level. Similar to fuel consumption of an internal combustion engine in a car, specific impulse is a measure of a rocket engines efficiency of thrust generation and is the most commonly used figure of merit when assessing a propulsion systems performance [11, 22].
Additionally, volumetric impulse ρI_{sp} can be used to evaluate propellant performance. It expresses the total impulse delivered per unit volume of the propellant and is defined by equation 2.6, where ρ is the propellants specific weight [22].

$$\rho I_{sp} = \rho \cdot I_{sp} \tag{2.6}$$

The volumetric impulse of a propellant gives an indication of the tankage and therefore structure mass that is required to carry a certain propellant. This is especially important if propellant tank space is limited, as is the case in satellites and scientific probes.

2.1.3 Liquid Monopropellant Rocket Engines

There exists a multitude of forms of rocket propulsion systems that can be classified on the basis of a wide range of criteria. One such classification can be done according to the type of energy source used in a given vehicle, that is chemical, nuclear or solar [11]. Of these the most commonly used are chemical rocket propulsion systems. These derive their energy from the high-pressure chemical combustion of propellants, usually a fuel and an oxidizing chemical. This reaction heats the reaction product gases to very high temperatures, after which the gases are expanded in a nozzle, accelerated to high velocities and ejected to generate thrust [11]. Chemical propulsion systems can be further classified according to the physical state of the propellant, mainly liquid or solid, although other systems exist, such as hybrid, combining both solid and liquid propellants components, gelled, or gaseous propellant systems that are less commonly used [11]. Within the context of this thesis only liquid propellant systems will be further discussed, as the others are not relevant when discussing green monopropellants. The basic components of a liquid propellant rocket engine are a thrust chamber comprised of the injector, nozzle and combustion chamber, propellant storage tanks and propellant delivery system components (e.g. pumps, valves, piping) [11, 20]. The propellant is fed, under pressure, from the tanks into the combustion chamber where the previously described chemical combustion takes place [20]. For small spacecraft propulsion systems the term thruster is commonly used to describe a small thrust chamber [11]. As mentioned in chapter 1 a common choice for in-space propulsion systems are monopropellant rocket engines, a class of liquid chemical propulsion system that, unlike bi-propellant systems, requires only a single propellant component. This results in a simpler system at the cost of lower performance. Figure 2.1 shows an example of one such thruster. While this specific thruster uses hydrogen peroxide as its propellant, this configuration is typical for SOTA monopropellant propulsion systems. Contained within the combustion chamber is the catalyst bed

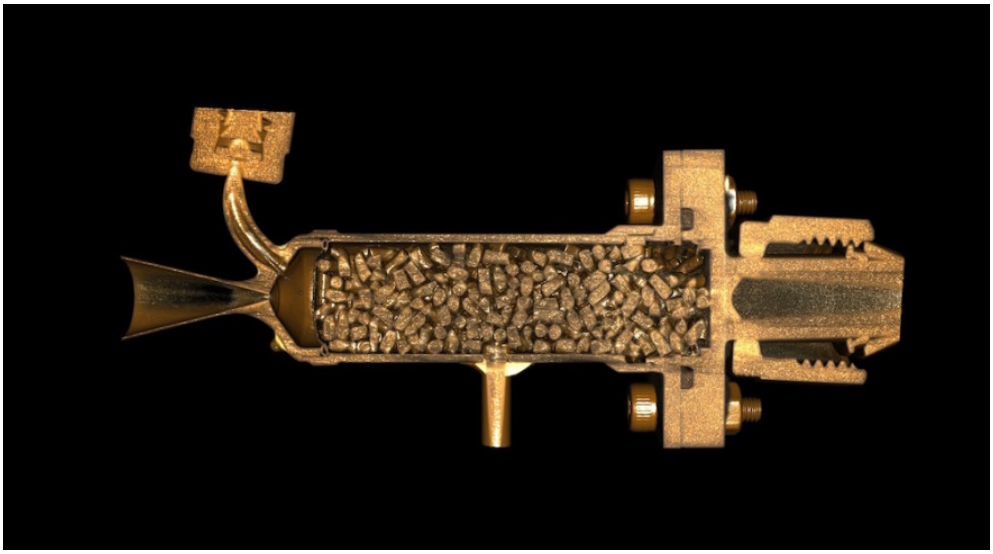

Figure 2.1: CT scan of a monopropellant thruster. The combustion chamber contains the catalyst bed used to initiated the exothermic decomposition reaction [23].

made up of granules of a catalyst material that initiates the propellants chemical decomposition

reaction on contact. This method of ignition is popular when it enables reliable spontaneous restart capability [1].

2.2 Green Monopropellants

Due to the drawbacks of hydrazine mentioned in chapter 1, interest in alternative monopropellants with equal or better performance than hydrazine has increased. The popular term to describe these alternatives is 'green monopropellants' [4, 5]. This description is misleading in the sense that the proposed alternatives aren't necessarily environmentally friendly, but refers mainly to the alternatives being non-toxic or less toxic than hydrazine [4, 5]. However, improved safety that goes along with a switch to greener alternatives is not the main driver for this trend, but rather a reduction of costs associated with propellant handling operations through simplification [24]. Yet low toxicity as such will not lead to an adoption of a proposed green alternative. Various factors need to be considered, of which system performance and overall reliability are key, if not the most important [24]. Multiple studies have sought to determine what qualifies a potential alternative as a green monopropellant and have attempted to define selection criteria or figures of merit by which they can be assessed and compared [4, 5, 24, 25]. These criteria can be summarized into three major categories:

- **toxicity:** High toxicity increases required personnel safety measures and potential environmental impacts.
- **handling & transportation:** Required costs and delays of ground operations significantly impact total costs and schedule.
- **performance:** Directly relates to size and mass and therefore cost of a spacecraft. Replacements should have the same or better performance characteristics compared to hydrazine.

Mayer and Wieling [5] based their definition of a green propellant on the Acute Toxicity Classification (ATC) of the Globally Harmonized System of Classification and Labelling of Chemicals (GHS). The classification of a substance ranging from 1 (most toxic) to 5 (least toxic) is based on the approximate lethal doses required to kill half of a tested population within a certain time by different means of administration of the toxic substance. Mayer and Wieling [5] classify a propellant as green if it falls in an acute toxicity class of 3 or higher. Other parameters such as carcinogenicity, mutagenicity and environmental impact are disregarded for the classification. The category handling and transportation consider, among other factors, the required PPE, operational constraints, shock sensitivity and pyrophoricity.

Performance is mainly evaluated by three parameters. Specific impulse (I_{sp}) and volumetric impulse (ρI_{sp}) both determine the size and mass of the required tanks and available Δv for a given mission. The third is combustion temperature, which determines what materials are required or whether cooling systems are a necessity. Additionally, ignition delay, pre-heat requirements and combustion roughness are included in the evaluation. State of the art hydrazine catalysts (e.g. Shell/S-405) do not require any pre-heat and are capable of reliable, repeated spontaneous starts

even at low temperatures [4, 26]. Finally, aspects such as operational lifespan and duty cycles are considered [4].

State of the Art Green Monopropellants

Current SOTA green monopropellants that fulfill the above mentioned requirements can be classified into three major categories, according to Nosseir et al. [25]:

- Energetic Ionic Liquids (EILs)
- Hydrogen Peroxide Aqueous Solutions (HPAS)
- Nitro Compounds (e.g. nitromethane)

In the following, a short background to each of these categories is given together with example propellants already introduced in figure 1.4, in order to asses how nitromethane compares to other, more matured, proposed green monopropellant, alternatives. Finally NM is discussed in more detail.

Energetic Ionic Liquids

EILs can also be described as premixed oxidizer/fuel ionic propellant blends [25]. The oxidizers are salts dissolved in aqueous solutions, called Ionic Liquids. These are mixed with Ionic Fuels or Molecular Fuels to form a premixed propellant. EILs can be further classified according to the Ionic Oxidizer used. Two popular choices for this are HydroxylAmmonium Nitrate (HAN) and Ammonium DiNitramide (ADN). An example of a HAN-based green propellant is SHP163, which was developed at the Institute of Space and Astronautical Science(ISAS)/(JAXA) and has already been tested in space as part of the RCS of the RAPIS-1 satellite launched by JAXA [25]. It has what is considered a high density of $1.4\frac{g}{cm^3}$ allowing it to achieve a high volumetric impulse of $\rho I_{sp} = 350\frac{gs}{cm^3}$. FLP-106 is a ADN-based monopropellant. Its development started at the Swedish Defense Research Agency (FOI) in 1997 and its use has also been demonstrated in space on the Mango-PRISMA satellite launched in June 2010 [25].

Hydrogen Peroxide Aqueous Solutions

Since 1938 hydrogen peroxide (H_2O_2) has been used as monopropellant in different in-space propulsion applications [25]. Classified according to its concentration, rocket grade high-test peroxide (HTP) is typically of 98% concentration [25]. While performance in terms of I_{sp} is lower than that of hydrazine, it boasts high density ($1.43\frac{g}{cm^3}$) and a lower combustion temperature (1225 K) than other green monopropellants [25].

Nitromethane

NM (CH_3NO_2) is an organic substance and a nitro compound with a single nitro group (N_2O). The greatest advantage over the other propellants previously discussed is the high specific im-

pulse. Its density of $1.14\frac{g}{cm^3}$ is higher than that of hydrazine yet lower than the above mentioned propellants. Some relevant properties of NM are summarized in table 2.1 taken from [10]. Based

Table 2.1: Nitromethane properties [10].

Property	**Value**
Formula	CH_3NO_2
Molecular Weight	61.04 g/mol
Density	1.137 g/cm^3
Melting Point	-28.83°C
Boiling Point (@atm)	101.19°C
Enthalpy of formation	-112.6 kJ/mol
Viscosity	0.630 mPa s

on the aforementioned criteria NM was identified by Mayer and Wieling [5] as the only suitable monopropellant of those reviewed in the study. EILs such as HydroxylAmmonium Nitrate (HAN) or Ammonium DiNitramide (ADN)-based propellants were considered unsuitable due to a low maximum specific impulse although, as mentioned above, the use many of these propellants has already been successfully demonstrated. In contrast, Mayer and Wieling [5] also note that neat NM is most likely unsuitable for use as a monopropellant for in-space propulsion systems when considering other factors not included in the selection criteria, such as its slow combustion rate and difficulty to ignite at pressure levels that are common for thrusters.
Table 2.2 contains an overview of the performance parameters of the propellants discussed above including hydrazine as a comparison. TODO: generate values using CEA with same condi-

Table 2.2: Green monopropellant performance parameters generated using NASAs CEA code. Input conditions: combustion at 10 bar, nozzle expansion ratio: 100, initial propellant temperature: 300 K; flow frozen at the nozzle throat. The parameters are theoretical vacuum specific impulse, density, volumetric impulse and combustion temperature.

Propellant	$I_{sp,vac}$[s]	ρ [$\frac{g}{cm^3}$]	ρI_{sp} [$\frac{gs}{cm^3}$]	T_C [K]
Hydrazine	202	1.00	202	875
SHP163	250	1.40	350	2256
FLP-106	243	1.40	340	2165
NM	266	1.14	303	2449
HTP 98%	175	1.43	250	1225

tions!

2.3 Previous Nitromethane Combustion Rate Studies

In the following section, research efforts and studies regarding the combustion rate of nitromethane are presented and discussed.

Generally the linear burning rate or combustion rate of a propellant is approximated as a function of chamber pressure [11]. The most commonly used form to describe this correlation is an empirical power law equation [11] shown in equation 2.7.

$$r_b = a \cdot p^n \tag{2.7}$$

With r_b as the combustion rate, usually in $\frac{mm}{s}$ and p as the combustion chamber pressure. a is the temperature coefficient, an empirical constant influenced by the ambient propellant temperature and n is the pressure exponent. The latter two values are determined by measuring combustion rates at different pressures and performing a power law regression analysis using the function defined above.

Early studies dating back to the 1950s conducted by Kindsvater et al. [12] aimed at improving NMs low combustion rate. The motivation behind this can be traced back to the correlation between a propellants combustion rate and its characteristic chamber length L^*. Essentially, this parameter is an indicator for the size of combustion chamber needed in order for a propellant to achieve complete combustion and in turn deliver good performance, before exiting the chamber [11]. It is a propellant-specific parameter that considers the time necessary for vaporization, activation and complete burning of the propellant [11]. These steps taken together are what make up the combustion process. Therefore, a higher combustion rate results in a lower characteristic chamber length and overall thruster size and consequently mass. The objective of the study was to determine methods of increasing combustion rates by use of additives or catalytic materials. Results showed that di-tert-butyl peroxide or chloral were most effective of the additives tested. Furthermore, it states that stainless steel is a specific catalyst for the thermal decomposition of nitromethane.

A widespread method of measuring combustion rates of liquid monopropellants are strand burners. Originally developed to obtain the combustion rate data for solid propellants, a strand burner is a small pressure vessel - usually optically accessible - in which a thin bar or cylinder of propellant, called a strand, is mounted on a stand, ignited on one end burned to the other end [11]. Chamber pressure is simulated by pressurizing the vessel with an inert gas and combustion rate is measured by electric signals from break wires embedded into the propellant strand [11]. For liquid monopropellants, the strand consists of a container - generally in tube shape - in which the propellant is loaded prior to testing.

Boyer [13] conducted combustion rate studies with NM using two different variations of a strand burner test stand. The first, named the Liquid Propellant Strand Burner (LPSB), was equipped with a propellant feed system that allowed long continuous test runs at pressures below 35 MPa. The combustion chamber was equipped with viewing windows to allow optical access and the usage of non-intrusive diagnostic techniques, rather than the aforementioned break wires. Nitrogen was used as an inert gas to pressurize the vessel. The propellant was fed into a quartz glass tube and ignited using a nichrome (NiCr) wire. An alternative method of containment was presented in the form of thin-walled cylindrical straws made from combustible wax in order to minimize heat loss and allow the propellant to burn at its intrinsic combustion rates. However, when comparing both methods negligible differences were observed. The combustion rate was measured using the

propellant feed system. It allowed precise adjustment of the feed rate so that the burning surface of the propellant could be stabilized at the tip of the tube. The combustion rate could then be derived from the set propellant feed rate. The second variation of a strand burner was named the Ultra-High Pressure Strand Burner (UHPSB) and was capable of testing at pressures up to 206 MPa. These tests were static, meaning that no continuous propellant feed system was used, but rather the propellant was loaded into one of the aforementioned containers and ignited at the top similar to the solid propellant strand burner. Tests at these pressures were conducted in order to assess the use of NM as liquid gun propellant. The study found that, the combustion behavior of NM can be divided into pressure regimes, with the lowest and the only relevant one for NMs application as a monopropellant for in-space propulsion systems ranging from 3 to 15 MPa.

Sabourin et al. [16] conducted strand burner tests in order to study the effect of additives on the combustion rate of NM. The setup used in this study consisted of a 316 stainless steel combustion chamber with a total free volume of 23 l and equipped with two opposed viewing windows. The high free internal volume of the chamber ensured minimal pressure variation due to the gaseous combustion products during a test run. Argon gas was used as an inert pressurant. The combustion process was recorded through one of the windows using a digital video camera, while the opposite window was backlit using an optical diffuser to ensure adequate lighting for the recording. From these recordings the combustion rate was determined. Similar to the previous study, the propellant was loaded into quartz glass tubes to enable observation of the combustion process.

In [8] a different, non-optical approach for the measurement of combustion rates was selected, whereby light intensity readings and pressure gradients were used to determine the moments of ignition and the end of burning. The focus lay on the pressure regime previously acknowledged by Boyer [13] and studied the effect of aluminum and silica nano-particles on the combustion rate of NM. Additionally, the the effect of different materials propellant container materials (quartz glass and carbon steel) were studied. The results reported showed that NM-based mixtures containing 1% SiO_2 and 5% Al lead to an increase in overall combustion rates and that carbon steel, due to a combination of heat transfer and active catalysis, likewise produced an increase in combustion rates. Unlike in the previously discussed studies, no inert gas was used to pressurize the combustion chamber. It was stated that the additional oxygen present in the air only influenced the reaction at its initialization. The rapid movement of the burning surface into the container prevented further access to the ambient oxygen, meaning that for the remainder of the test the NM burned as a monopropellant. Furthermore, the presence of ambient oxygen aided in the ignition of the NM.

Derk [14] used a similar setup to those mentioned above. Borosilicate glass (BSG) tubes with varying diameters were used in order to also study the effect of tube diameter on NM combustion behavior. It was found that for the diameters tested (between 1 and 14 mm) tube diameter had no effect on the combustion rate in the low pressure regime <18 MPa. These results matched the findings of another study by Sabourin et al. [17]. Measurement of the combustion rate was accomplished using a HS-camera and an image processing tool written in MATLAB to determine combustion rates from footage.

A different method of measuring the combustion rate of nitromethane was demonstrated in a thesis completed at DLR by Ziemer [27]. In this study propellant droplets were suspended from a small glass rod and ignited using a glow plug. Similar to the above mentioned studies, difficulties igniting neat NM were reported to the extent that only by the addition of additives could ignition be achieved. This behavior was also reported in all of the above mentioned studies. To address this, the solid booster pellets were added to aid in the ignition of NM at pressures below 4.5 MPa.
Table 2.3 summarizes the experimental methods applied in the above mentioned strand burner studies.

Table 2.3: Overview of previous NM combustion rate studies and their applied methods.

Source	[13]	[16]	[8]	[14]
Type	fed, static	static	static	static
Container	tube, straw	tube	tube, cavity	tube
Material	quartz, wax	quartz	quartz, steel	BSG
iD [mm]	7	8	7	10.6
L [mm]	65	70	-	100
Ignition	NiCr wire, solid booster	NiCr wire, solid booster	NiCr wire, solid booster	NiCr wire, solid booster
Measurement	feed rate, HS-cam	HS-cam	light intensity, pressure	HS-cam
r_b	$0.173 \cdot p^{1.17}$	$0.162 \cdot p^{1.23}$	$0.165 \cdot p^{1.22}$	$0.183 \cdot p^{1.15}$
p [MPa]	3<p<15	3<p<10	3<p<13	3.6<p<18.2

2.4 Propellant Additives

Multiple studies have shown that the use of additives delivers favorable results on the combustion behavior of nitromethane. In this section, the additives that were selected for this thesis is introduced.

In a thesis by Ziemer [27] where NM combustion rates were obtained in droplet combustion tests, catalytic additives were shown to have positive effects on both combustion rate and ignitability of NM. The first of these was chromium(III) acetylacetonate (CAA) which has already seen use as an additive for NM in the past by Aerojet to address ignition and combustion stability concerns, resulting in the mixture known as 'Neofuel' [19]. The second additive was an iron-based organometallic compound (OMC1).

To address the high shock sensitivity of neat NM, studies conducted at DLR identified n-butanol (BUT) as an effective means of inhibiting detonation reactions to an acceptable degree [10] while ongoing research being conducted by the same party has identified an organosulfur compound (OSC1) that promises to deliver equally favorable results.

The thermochemistry data required for computing performance parameters of NM-based mixtures containing these four additives is listed in table 2.4. The values for OMC1 and OSC1 were provided by DLR. The remaining values were taken from [28] Using these values, performance parameters

Table 2.4: Thermochemistry data of the propellant additives. ρ is the density and $\Delta_f H^\circ$ is the enthalpy of formation [28].

	ρ $[\frac{g}{cm^3}]$	$\Delta_f H^\circ$ $[\frac{kJ}{mol}]$
OMC1	1.11	158
CAA	1.34	-366
OSC1	1.10	-203
BUT	0.81	-327

can be calculated using the NASA CEA code. The results of the calculations are listed in table 2.5.

Table 2.5: Mixture performance parameters calculated using CEA. Input conditions: combustion at 20 bar, nozzle expansion ratio: 100, initial propellant temperature: 300 K. Density was calculated using additive properties in table 2.4.

Mixture	$I_{sp,vac}$ [s]	ρ $[\frac{g}{cm^3}]$	ρI_{sp} $[\frac{gs}{cm^3}]$	T_C [K]
neat NM	269	1.14	306	2454
1OMC1	266	1.14	304	2397
2OMC1	264	1.14	301	2346
2CAA	266	1.14	304	2392
13OSC1	248	1.13	282	1977
6BUT	253	1.12	283	2028
10OSC1OMC1	251	1.14	285	2034
13OSC12OMC1	242	1.13	275	1897
13OSC12CAA	246	1.14	280	1917
6BUT2OMC1	248	1.12	278	1922
6BUT2CAA	250	1.12	281	1966

3 Experimental Setup

In this chapter the experimental setup that was developed as part of this thesis is introduced and discussed. First, requirements are defined based on the thesis task description followed by a discussion regarding design choices of some key features. The resulting design is presented by means of 3D CAD models. Following this the piping and instrumentation and control and data acquisition systems are presented. Finally, the image analysis tool used to determine the combustion rate is presented including an estimation of the measurement error for this method.

3.1 Requirements

The requirements for the experimental setup were derived from the task description and are listed in table 3.1. The process of requirements definition is based on ECSS standards [29]. Following these standards requirements denoted with an 'F' indicate a functional requirement that defines what the setup shall perform and those denoted with a 'D' indicate a design requirement that is related to imposed design and construction standards with regards to choice of components, design standards and safety considerations. The primary goal of the design is to enable the controlled

Table 3.1: Requirements.

ID	Description
F.1	The setup shall be able to hold, ignite and burn a liquid, viscous or gelled propellant strand or column, i.e. a volume of propellant held in a container in such a way that it can be ignited on one end (top) and burn to the other end (bottom).
F.2	The setup shall enable ignition and combustion in a chemically inert atmosphere at constant pressures up to 6.0 MPa by means of a pressure vessel.
F.3	The setup shall allow optical access to the propellant strand or column meaning both the container and the pressure vessel shall allow optical observation of the ignition and combustion processes.
F.4	The setup shall enable the measurement of the propellant combustion rate.
D.1	The means of ignition shall be characterized with a variable and well-defined ignition temperature or energy.
D.2	At no point during preparation, execution or follow up of the experiments shall the user or observers be exposed to any risk of harm.

burning of a propellant in such a way that the burning rate can be measured as stated in F.1 and F.4. Additionally, F.3 states that the process should be observable by means of an optical

access to allow the use of optical methods of measurement. Since the setup is to be used for studies of monopropellants for in-space propulsion applications the conditions at which ignition and burning takes place must be representative for these applications. F.2 therefore states that combustion must take place in an inert atmosphere and at chamber pressures typically reached in monopropellant thrusters during operation (1.0-4.0 MPa).

To enable comparison of ignition behavior between propellants and propellant mixtures, characterization of the ignition method is necessary, as stated by D.1. D.2 addresses safety considerations. Operation of the experimental setup will involve high pressures, hazardous chemicals and their combustion. Because of this there exists a high potential of harm which must be mitigated through adequate safety features and handling procedures.

3.2 Design Description

In the following section the design process for the main components of the strand burner test stand is presented.

3.2.1 Chamber design

Igniting and burning a propellant at elevated pressures in such a way that it can be observed visually requires a combustion chamber with optical access. Such a chamber was previously designed, manufactured and successfully used at the DLR. It was initially designed for studies involving gelled propellants by Kir [30] but was more recently adapted by Ziemer [27] to conduct droplet combustion experiments. Having been successfully used in the past this design is proven. Additionally, all necessary hardware has already been purchased and or manufactured and is stored at the DLR. For these reasons this design will act as the baseline for the experimental setup of the present work.

3.2.2 Pressure regulation

The combustion rates are to be determined at specified pressure levels. Therefore, pressure must remain constant during a single test run. Exhaust gases generated by the combustion would however, lead to a rise in pressure. This pressure increase must be addressed by some means. In previous studies different methods of achieving this have been implemented. In [14] electrically actuated needle valves were used to control the gas flow to and from the combustion chamber. Gudnason [31] used an adjustable proportional pressure relief valve to expel the combustion products. Both of these methods require either active control during a test in the case of the needle valves or repeated adjustment when varying chamber pressures between tests. The first method additionally adds complexity to the system. Another method that was not considered due to its complexity would be to actively regulate pressure using a controller. A different approach was chosen for this work. In [32] the chamber dimensions, and consequently the free volume, are large enough that pressure variation due to the gaseous combustion products is minimal. As the

dimensions for the selected combustion chamber are fixed, a pressure vessel is added to achieve the same result. To verify that the pressure gain does not exceed a set limit for a given pressure vessel the total pressure of the gaseous exhaust products must be calculated. This can be done using the NASA Chemical Equilibrium with Applications (CEA) code [33] to calculate the molar mass of every species present in the combustion products. An assigned-temperature and assigned-pressure problem with pure nitromethane as the reactant is used for this purpose, with pressures ranging from 5 bar to 50 bar and temperatures set such that all exhaust products are present in gaseous form. The calculation is done for an initial estimate of $V_{NM} = 2ml$ of NM. The CEA code produces the results listed in table 3.2. Using these values the partial pressure of a given

Table 3.2: Results of NM assigned-temperature and assigned-pressure problems calculated with the CEA code. Mole fractions of combustion products for set initial pressures. The temperatures after the reaction has taken place were chosen so that water has not yet condensed to a liquid and no soot formation has occurred so that all of the exhaust products listed are present in gaseous form.

p [bar]	5	10	20	30	40	50	60
T [K]	950	950	950	1000	1000	1000	1000
species	mole fractions						
CH4	0.039	0.063	0.086	0.074	0.083	0.090	0.096
*CO	0.130	0.105	0.081	0.102	0.091	0.084	0.078
*CO2	0.192	0.209	0.225	0.208	0.215	0.220	0.244
*H2	0.252	0.206	0.162	0.175	0.157	0.144	0.134
H2O	0.207	0.229	0.251	0.249	0.258	0.264	0.269
*N2	0.180	0.188	0.195	0.191	0.194	0.196	0.198

species p_i in the exhaust can be calculated using the ideal gas law in equation 3.1 [34].

$$p_i = \frac{n_{NM} \cdot X_i \cdot R \cdot T}{V_{tot}} \tag{3.1}$$

Where n_{NM} is the amount of substance of nitromethane, X_i is the species mole fraction, the ideal gas constant is $R = 8.314\frac{J}{K \cdot mol}$ [34], T is the assigned temperature and V_{tot} is the total free volume of the experimental setup. This in turn is calculated as by summing up the chamber and pressure vessel volumes as shown in equation 3.2.

$$V_{tot} = V_C + V_{PV} \tag{3.2}$$

with $V_C = 516cm^3$ as the combustion chambers internal volume and $V_{PV} = 7069cm^3$ as the pressure vessels internal volume. The latter is taken from a diving cylinder that was previously used as a fluid tank and was readily available at DLR. As a simplification the enclosed volume of the piping is disregarded for this calculation. The results of these calculations done for each species at each pressure level is listed in table 3.3. The maximum pressure increase $p_{ex,max} = 0.41bar$ falls within the measurement uncertainty of typical pressure sensors (1 bar) that are suited for the current application [35]. Additionally, this assumes that the entire amount of propellant is burned instantly and temperatures within the pressure vessel reach the assigned temperature. Therefore this value for $p_{ex,max}$ can be considered a conservative estimate.

Table 3.3: Partial pressures of pure NM combustion products calculated using CEA output in table 3.2.

p [bar]	5	10	20	30	40	50	60
T [K]	950	950	950	1000	1000	1000	1000
species	partial pressures [bar]						
CH4	0.015	0.024	0.033	0.030	0.034	0.037	0.039
*CO	0.050	0.040	0.031	0.041	0.037	0.034	0.032
*CO2	0.074	0.080	0.087	0.084	0.087	0.089	0.091
*H2	0.097	0.079	0.062	0.071	0.064	0.058	0.054
H2O	0.080	0.088	0.097	0.101	0.105	0.107	0.109
*N2	0.069	0.072	0.075	0.078	0.079	0.080	0.080
total	0.385	0.385	0.385	0.405	0.405	0.405	0.405

3.2.3 Ignition method

As stated in chapters 1 and 2 it is difficult to initiate combustion of neat nitromethane, specifically at those pressures that are relevant for studies to be conducted in the course of this work. The most common method used was a NiCr wire heating element [13, 8, 14, 16], either coiled or uncoiled, that was dipped into the NM. At lower pressures this was supplemented by a solid booster pellet threaded onto the wire. One study was found where ignition was achieved without the aid of booster pellets using only the wire wrapped around the tip of the tube holding the propellant [36]. More modern ignition techniques using resonant lasers were briefly mentioned but not implemented in [15]. Due to the high complexity of such a system and the fact, that its use was not proven within the mentioned study, methods such as these are not considered for the present work. In [27] a glow plug was used to ignite NM-droplets but this was not successful for neat NM only with mixtures containing catalytic additives. Figure 3.1 offers an overview of the methods that were considered for the present work. The first four methods shown in figures 3.1a through 3.1d all involve the use of nichrome wire, either straight (3.1a), coiled (3.1b), with a solid booster threaded on (3.1c) or wrapped around the tip of the tube (3.1d). This means that the ignition system as a whole can be designed in such a way that it is possible to switch between methods without making any further changes to the system. This provides some flexibility during testing if issues regarding ignition are encountered. The fifth option, shown in figure 3.1e, is the aforementioned glow plug method.

To decide which of the methods depicted is most suitable some preliminary ignition tests using neat NM were conducted. Figure 3.2 shows an example of one such test for the method using a coiled nichrome wire dipped into the glass tube holding the propellant. Similar setups were used to test the other ignition methods including the glow plug method. It was also opted against testing the method involving the solid booster pellet as it was deemed a proven method, having seen extensive use in the studies referred to above. The tests were conducted in air at atmospheric pressure since at this stage in the development process the combustion chamber and fluid systems had not yet been completed. Ignition was successfully achieved using the nichrome wire methods with methods (b) and (d) producing the best result, that is igniting the propellant the fastest. Furthermore, the technique of wrapping the wire around the tip of the tube holding the propellant appears

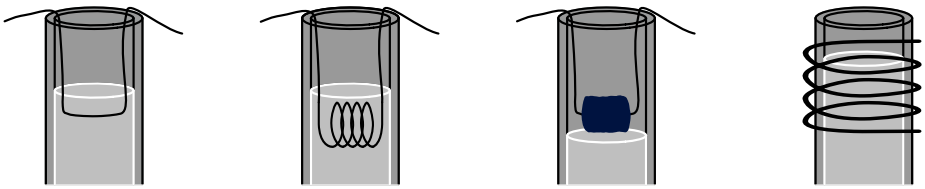

(a) Straight wire [13, 8].

(b) Coiled wire [16]

(c) Solid booster [13, 14, 16, 8]

(d) Tip coil [36].

(e) Glow plug [27].

Figure 3.1: Ignition methods from previous studies that were considered for this work.

very promising having been proven successful both in previous studies [36] and in the preliminary tests. If this method can be successfully applied in the finished setup, solid boosters would be unnecessary even at lower pressures, resulting in a simpler design. The glow plug method was not capable of igniting the propellant. While the glow plug method proved unsuccessful in these preliminary tests, additional reasons made this option impractical. As shown in figure 3.1e the glow plug would need to be inserted into the tube from above to enable ignition from the top. This would leave the tip of the glow plug hanging above the flame during combustion where it would experience temperatures significantly greater than the typical operating temperatures of a glow plug which lie at 1400°C in comparison to the combustion temperature of neat NM at 2200°C (see table 2.5 for value in K). In order to not destroy the glow plug it would need to be retracted after ignition, greatly increasing complexity of the design compared to the nichrome wire method. Based on these results methods (b) and (d) are selected as the ignition methods for the strand burner test stand.

3.2.4 Measuring Combustion Rate

The traditional way of measuring combustion rate is using break wires that, as the flame progresses through the propellant strand, would break, interrupting the signal being passed through the wire and indicating the position of the flame at the signal loss [13, 37]. Using multiple wires at known positions could then be used to determine the combustion rate. However, a system like this would involve considerable effort in test preparation. Most modern strand burner setups make use of optical measurement techniques where the high-speed (HS) imaging is used to record the combustion process. The recorded footage can then be analyzed either visually by hand or by use of image analysis tools. McCown et al. [8] opted for a different, non-optical approach. Instead, light

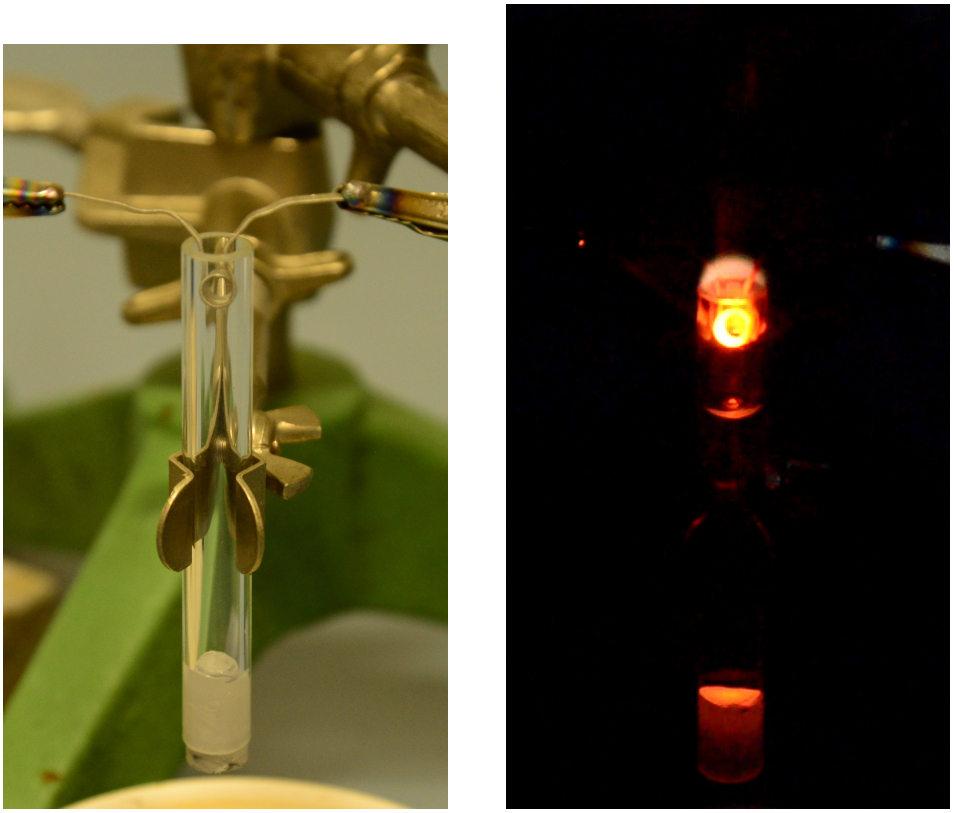

Figure 3.2: Image taken during one of the preliminary ignition tests conducted as part of the ignition method selection.

intensity was measured indicating the time of ignition and the moment the flame expired. Pressure readings were used to verify the light intensity readings by identifying positive pressure gradients as the moment of ignition and negative gradients for the end of burn. This method was not considered as the requirements call for an optically accessible setup making light intensity readings impractical. Furthermore, the select pressure regulation method presented above seeks to minimize pressure variations during combustion making it difficult to detect beginning and end of burn from pressure readings. Therefore, measurement of combustion rate by use of HS imaging is selected for this work. A image analysis tool was implemented in Python using the Open Source Computer Vision Library (OpenCV) library as it offers a wide range of image processing functions and an abundance of resources available online without additional cost. Furthermore, this approach was successfully applied in the previous work completed at DLR by Ziemer [27].

3.2.5 Safety considerations

To ensure that no human is exposed to any risk of harm during operation of the setup, as stated in the requirements, a control system will enable remote operation of critical functions. These are pressurization, pressure release and ignition. Furthermore, the fluid system will be designed in way such that mechanical or electrical failures do not result in an unresponsive and unsafe system.

3.3 Design Summary

In this section the final design that was developed based on the presented requirements and the results of the discussion will be presented.

Figure 3.3 shows the full assembly of the combustion chamber in a cut isometric view and a cut front view. It is comprised of the combustion chamber itself with a stainless steel core, a front and rear window assembly and the strand plug framed in green, which is also made of stainless steel. The window assemblies each consist of a sapphire glass window held in place by a pair of stainless steel frames (inner and outer). The window is sealed off using two graphite gaskets, between the window and inner or outer frame, respectively. A total 16 M6 bolts clamp the inner and outer frame together creating the seal. An additional gasket is placed in between the inner frame and the chamber core. Another 16 M6 bolts are used to clamp the two components together. As mentioned in the previous section, the combustion chamber design was adapted from previous work and the hardware was reused, hence the multiple plugs used to seal off ports that are not required for this work. Modifications were made in two positions: a large bore was added to the bottom face of the chamber core in which the strand plug is inserted and an access port was added to the top face through which propellant is loaded into the tube. Two ports in the chambers left and right walls act as gas inlet and outlet. An enlarged view of the strand plug is displayed in

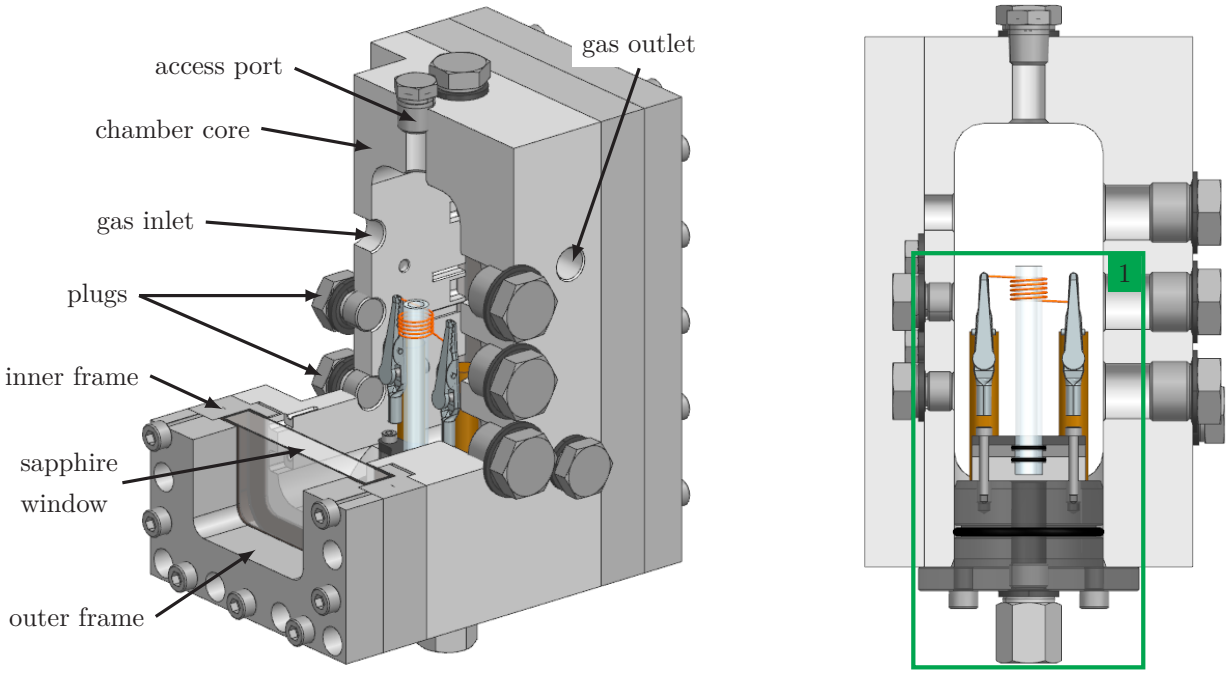

(a) Isometric view.

(b) Front view with strand plug.

Figure 3.3: Isometric and front view of the combustion chamber assembly. Sapphire windows in front and back allow optical access to the interior. The strand plug is highlighted by the #1 green square.

figure 3.4. It is mounted into the chamber core via a flange and fastened using four M6 bolts. An

o-ring is used as a seal between the chamber core and the strand plug. As a means of holding

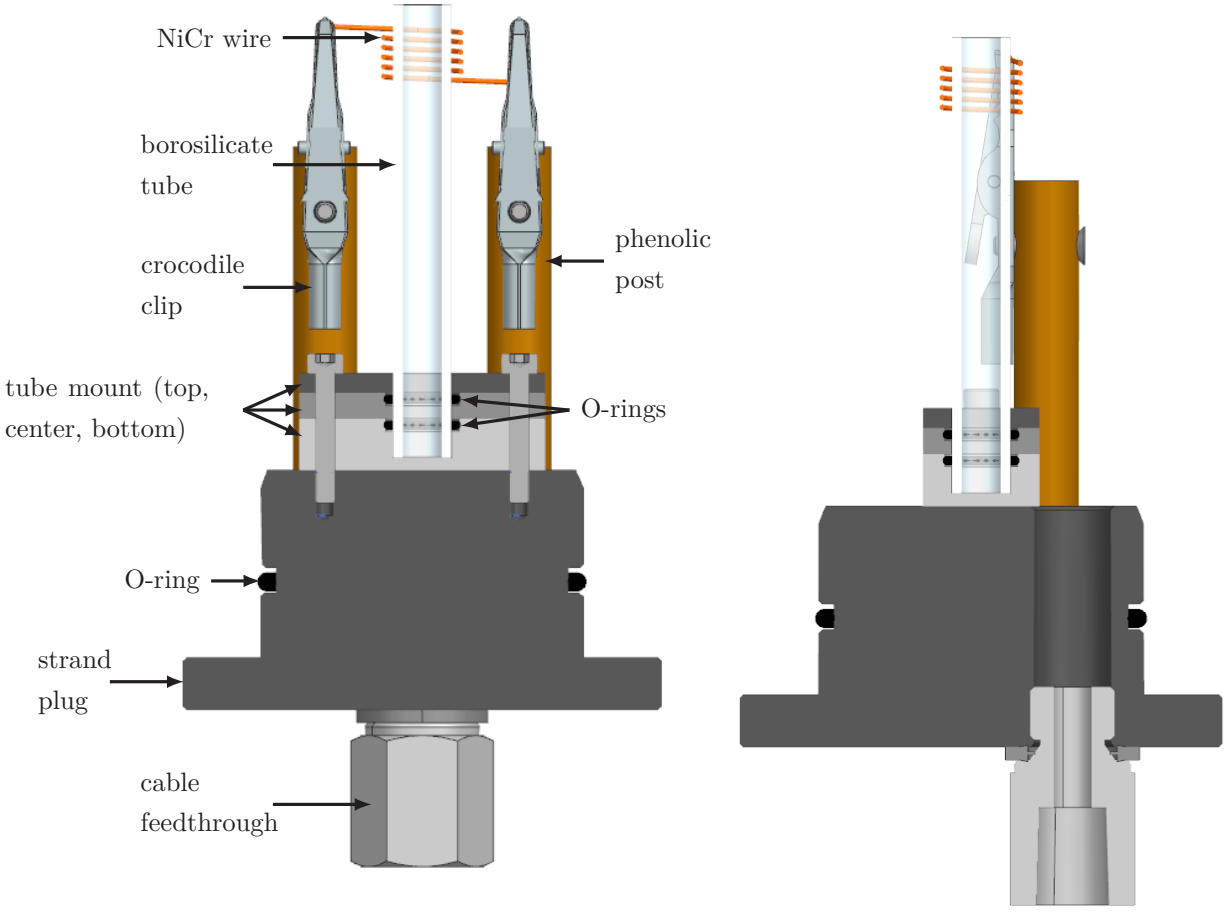

(a) front view (b) side view

Figure 3.4: Front cut view and side cut view of the strand plug that is inserted into the combustion chamber.

the propellant such that the combustion process can be observed a borosilicate glass tube with an outer diameter of 9 mm, an inner diameter of 6 mm and a length of 70 mm is used. The tube is held in the tube mount, three machined aluminum plates with through holes in the top and center element and a blind hole in the bottom plate, and its bottom is sealed with two o-rings. The tube mount is fastened onto the strand plug using two M3 bolts. Two phenolic posts that are equipped with threads glued into their bottom faces are also mounted onto the strand plug. These are used to support and isolate the ignition system. A pair of crocodile clips are fastened to the phenolic posts with screws and hold the nichrome ignition wire. In this image the version of the ignition system where the wire is wrapped around the tip of the tube is displayed as an example. The power for the ignition system is supplied via the pressure tight cable feedthrough insert which is modeled as pressure fitting as a placeholder. The two ignition wires, equipped with ring terminals on their ends, are fed through the bore in the strand plug and fastened with the same screws used to fasten the crocodile clips.

3.3.1 Piping and Instrumentation

In order to pressurize the system to the desired pressure levels a fluid system was designed with a focus on safety, ease of operation and simplicity. The fluid system is presented with the aid of the piping and instrumentation diagram (P&ID) shown in figure 3.5. The system is divided into two sections: the supply line and the exhaust line. They connect to their respective ports in the combustion chamber with the supply line feeding into the gas inlet port and the exhaust line connecting to the gas outlet port. To simulate conditions representative for those present in monopropellant thrusters an inert gas is used to pressurize the chamber. As it is readily available, nitrogen was selected for this purpose. It is supplied from a 50L, 200 bar gas cylinder. The gas is then fed into a pressure regulator valve 1PR1 used to set the desired pressure. The valve is equipped with a pressure gauge that measures and displays the valve outlet pressure mechanically on a dial. This device offers no method of reading the set pressure in a precise manner. It will therefore only be used to set the pressure to roughly the desired level. The line then feeds into the pneumatically actuated ball valve 1V1 which is opened to pressurize the chamber. A solenoid valve controls the pneumatic actuator remotely via an electric signal. A normally closed valve was chosen for this application in order to seal off the chamber in case of a failure rendering the valve uncontrollable. Finally, a check valve 1C1 prevents backflow. As a safety feature in case of a failure of the pressure regulator valve, a pressure relief valve 1R1 is connected to the supply line behind 1PR1 via a T-junction. It is set to open at 75 bar. When gases exit the chamber into the

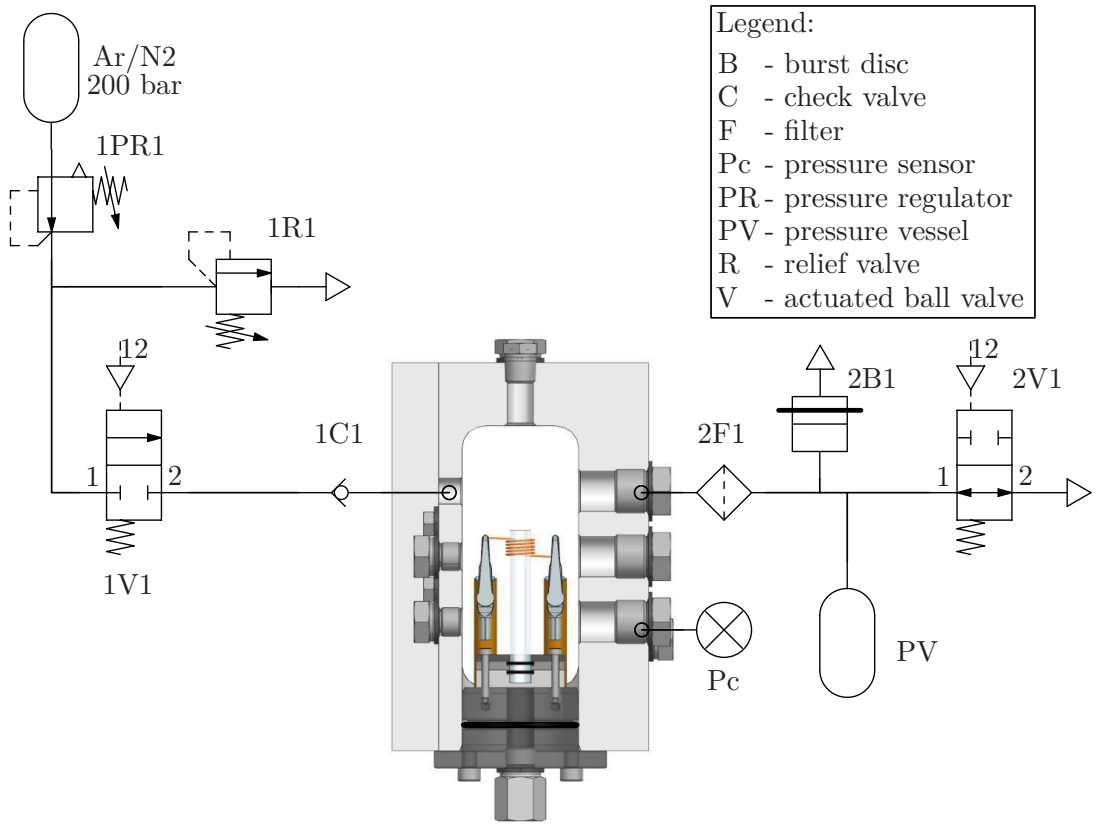

Figure 3.5: P&ID of the strand burner test stand.

exhaust line they are first fed through a filter 2F1 to catch all solid exhaust products, such as soot, and prevent these from being expelled into the working area. A T-junction divides the line on the path leading into the pressure vessel PV, and the other continuing to the second actuated ball valve 2V1. This valve serves as the pressure release valve. When it is opened gases are expelled into the surrounding which must be considered when deciding where to place the setup. Valve 2V1 is a normally open valve. This ensures that the system automatically returns into a safe state in the case of a valve or valve control failure. This is necessary as the check valve prevents a pressure release through the supply line. For the same reason an additional safety feature was added via a second T-junction in the form of a bust disc 1B1. While it is non-reusable, a burst disc provides greater protection from sudden pressure surges. A relief valve opens with some delay. During this time the combustion chamber could experience pressures greater than that which it was designed for. The burst pressure of the selected discs is 75 bar.
A pressure sensor P_C is directly connected to the combustion chamber. A WIKA model A-10 pressure transmitter with a measuring range of 0 to 100 bar and an output of 4 to 20 mA [35].

3.3.2 Ignition System

The ignition system is comprised of a power supply unit connected to the nichrome wire via crocodile clips and the cable feedthrough. It functions by resistance heating the wire by passing a current through it. A requirement was defined in table 3.1 which states that the means of ignition shall be characterized with a defined ignition temperature or energy. Two methods were considered determine the wire temperature as a function of the supplied current.

The first is to measure the resistance of the wire using the 4-wire or 4-probe resistance measurement method [38] and use the correlation between resistance and temperature of an electrical conductor defined in equation 3.3 taken from [39].

$$R = R_0 \left(1 + \alpha \left(T - T_0\right)\right) \tag{3.3}$$

R_0 is the resistance at the reference temperature, T_0, which is usually 20°C. α is the temperature coefficient, which is a material property and can vary depending on the purity of the material. This issue was abandoned for two reasons. The first is connected to the aforementioned temperature coefficient α. Since it is greatly dependent on the quality of the material and varies widely from one source to another (see [38, 39] and needs to be provided by the wire manufacturer. However, for wire used in this work the manufacturer provided only discrete values for temperature at a given set current and not the temperature coefficient [40]. The second reason that made this method unfeasible is that the hardware required for the resistance measurement was not available at DLR and could not be purchased due to its high cost.

The second method is to directly measure wire temperature using a thermocouple. This was attempted by connecting the thermocouple to the wire using a thermocouple welder. However, due to the high temperatures to which the wire is heated to ignite the propellant the weld joint would already fail during heating. Therefore, this method was also abandoned.

It was finally decided to rely on the data provided by the manufacturer mentioned above. With this the temperature can be estimated using the current value set on the power supply unit. The ignition energy can be determined by visually observing the voltage output of the power supply unit and then calculating the energy using equation 3.4 taken from [39].

$$E = P \cdot t = (I \cdot V) \cdot t \tag{3.4}$$

With t as the time between activation of the power supply and ignition, P as the electric power, I as the current and V as the voltage.

3.3.3 Control and Data acquisition

The purpose of the control and data acquisition system is to enable a remote controlled operation of the entire experimental setup. For this a system was designed that allows opening and closing of the valves and triggering the ignition system and HS camera recording. Additionally, it is capable of reading and converting the pressure transmitter output and storing the data. The complete experimental setup is shown in figure 3.6 as a schematic. The strand burner including

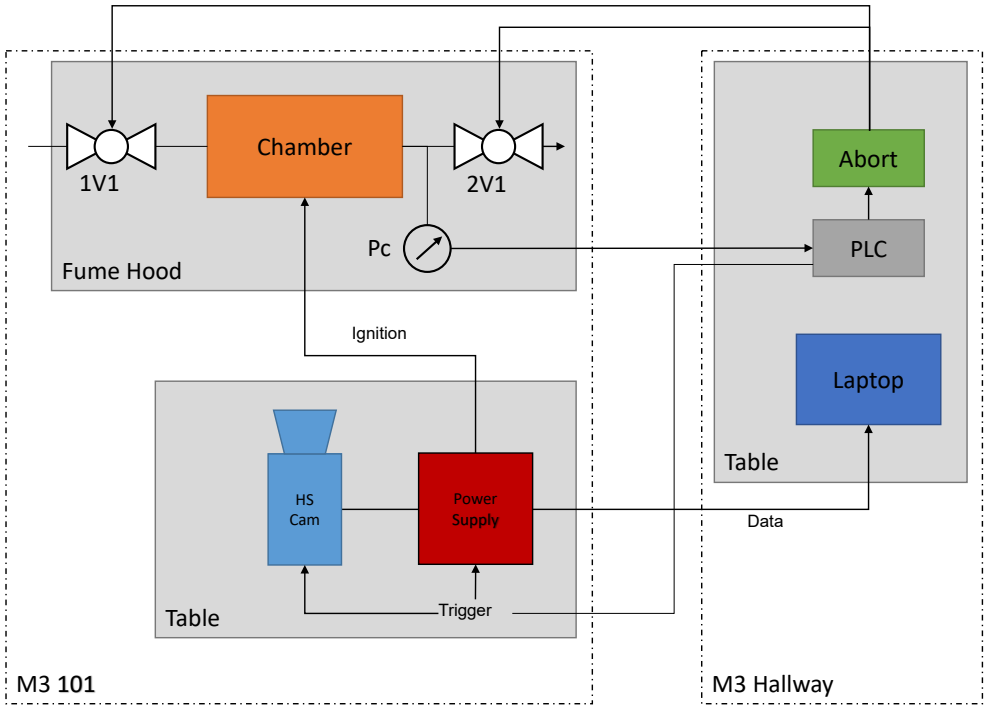

Figure 3.6: Schematic of the experimental setup.

the fluid system is placed inside a fume hood. This ensures that exhaust gases are immediately extracted and not released into the work area. The HS camera and ignition system power supply are placed on a table in front of the fume hood. The camera model used is a Photron Fastcam SA-X2 and the power supply is a Basetech BT-3020 Bench PSU. The power supply output is connected to the cable feedthrough in the strand plug. The system is controlled from outside the room in the hallway where a laptop and the programmable logic controller (PLC) are placed on

a table. The HS camera is connected to the laptop. It is controlled using the viewing software provided by the manufacturer (Photron Fastcam Viewer 4). The PLC unit is a PiXtend V2 -L-, a microcontroller connected to a Raspberry Pi single-board computer. A separate power supply is integrated into the unit which delivers power to the solenoids controlling the pneumatic actuators for the valves. The PLC allows the control of multiple digital output signals and relays and is capable of reading various analog and digital input signals. Output signals are used to control the 1V1 and 2V1 solenoids and to send trigger signals to the HS camera and the ignition power supply in order to activate the recording and ignition system, respectively. An emergency stop switch is hardwired to the solenoid power supply and the ignition trigger signal to allow a redundant non-software abort at any point during operation. The pressure transmitter signal is fed into one of the analog inputs of the microcontroller. Additionally, a thermocouple can be connected to the PLC. Its signal is first fed into a thermocouple measuring transducer to configure the measuring range. The resulting signal is then connected to one of the analog inputs of the microcontroller. The microcontroller is operated via the Raspberry Pi using a graphical user interface (GUI) that was implemented in Python. A screenshot of this program is shown in figure 3.7. In the top

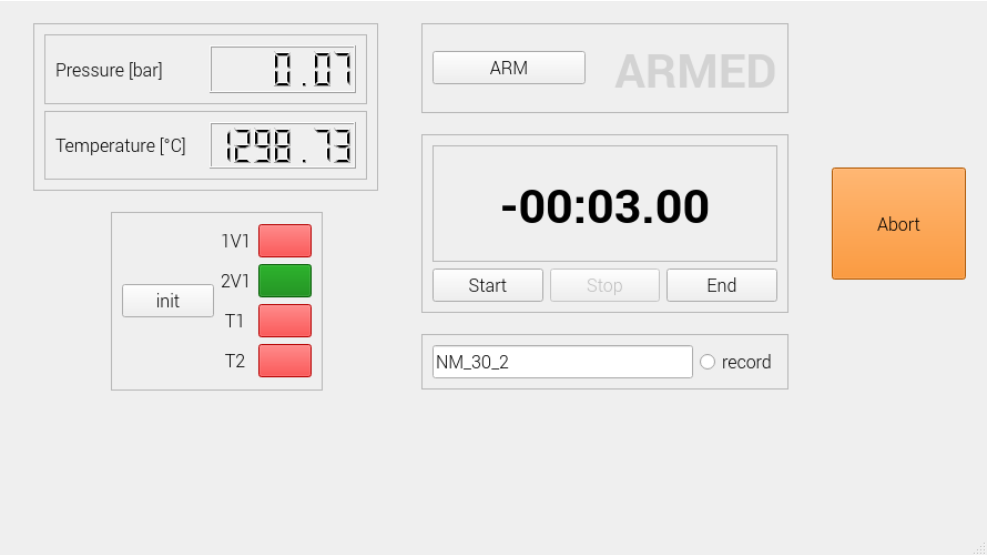

Figure 3.7: Screenshot of the controller GUI. All output signals (triggers and valves) are in their initial state and the system is unarmed.

left corner the pressure and temperature readings are displayed. The buttons positioned below this allow the manual control of all output signals. The buttons are colored to indicate either the valve position (green = open, red = closed) or the trigger signal states (green = active, red = disabled). The 'init' button activates the microcontroller enabling sensor readings and output signal control. Arming the system is done by clicking the arm/disarm switch located in the top center section of the GUI. Below this the countdown timer is located together with the 'START' and 'STOP' buttons to initiate or end the test sequence. Both the trigger signals and initiation of the test sequence can only be clicked when the system is armed to avoid accidental activation. Initiating the control sequence disables manual control of the output signals to prevent accidental button presses. 'STOP' re-enables manual control after a test run is complete. The 'END' button

disables the microcontroller disabling all output signals and ending sensor readings. At the bottom center of the GUI the user can decide whether sensor readings are stored during a test sequence by toggling the 'record' button. If active an output file is generated with the test run name or ID that was entered in the text input field before initiating a test run. A software abort button is located on the right side of the GUI. Clicking this at any point in time before or during a test run disables all output signals but does not terminate the timer or data recording. The system is returned into its initial state with 1V1 closed, 2V1 open and both trigger signals disabled. After aborting, manual control of the valves is re-enabled.

Control sequence

Once the system is armed pressing the 'START' button initiates the test control sequence:

1. If not already the case, valves 1V1 and 2V2 are closed and manual control of all output signals is disabled.
2. Data recording is initiated.
3. Countdown start at T -3.0s.
4. At T -2.0s trigger signal T2 is enabled to start HS camera recording.
5. At T -0.0s trigger signal T1 is enabled activating the ignition system power supply.
6. This state is maintained until the sequence is ended by pressing the 'STOP' button, or else, in case of emergency, the test is aborted.

4 Testing Procedure

In this chapter the testing procedure is described along with some key components and features of the setup in order to demonstrate how the design presented in chapter 3 was realized. Finally, the test plan that served as a starting point for both test campaigns is introduced, including the additives that were selected to be tested.

4.1 Test Preparation

Prior to testing various steps were completed beginning with the preparation of the borosilicate glass tubes shown in figure 4.1, which are used to hold the propellant during test runs. The tubes

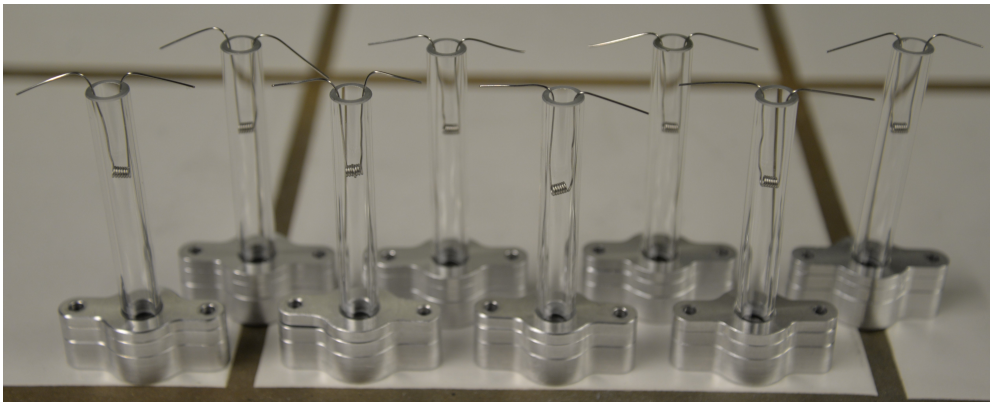

Figure 4.1: Borosilicate glass tubes inserted into the tube mounts in preparation for strand burner tests. NiCr ignition wires coiled and cut to length have already been inserted into the glass tubes.

are inserted into the tube mounts, which serve the additional purpose of sealing off the bottom of the tube using o-rings. Finally, the ignition wires are inserted into the tube. The wire used is an Omega 0.51 mm diameter, 80% nickel 20% chromium resistance heating wire [40]. It was delivered in spools and had to be coiled and cut to the desired length, depending the position, or depth, within the tube at which the coil should hang. A COTS coiling tool was used to give each wire a coil with an inner diameter of 1.5 mm and seven turns. The lead ins were then bent at the distance from the coil that corresponded with the desired coil depth. The value for this parameter would be determined during the run-in test campaign and selected for all following tests. This ensured that wire length, and in turn wire resistance was sufficiently similar for each test. The coiled and bent ignition wires were then placed into the prepared glass tubes. To allow for more time-efficient operation a set of eight of the assemblies shown in figure 4.1 were prepared at once. As mentioned in chapter 3, two methods of ignition were selected. However, early tests with the completed setup showed that the method, for which the wire is wrapped around the tip of the

tube, could not ignite the propellant and in the following tests only the other method selected was used. This will be further elaborated upon in chapter 6.

For a test run a glass tube was placed onto the strand plug, as shown in figure 4.2, and fastened with two screws. This ensured that for every test the glass tube was in the same position, meaning no readjustment of the camera orientation was necessary. Finally, the wire leads were fastened

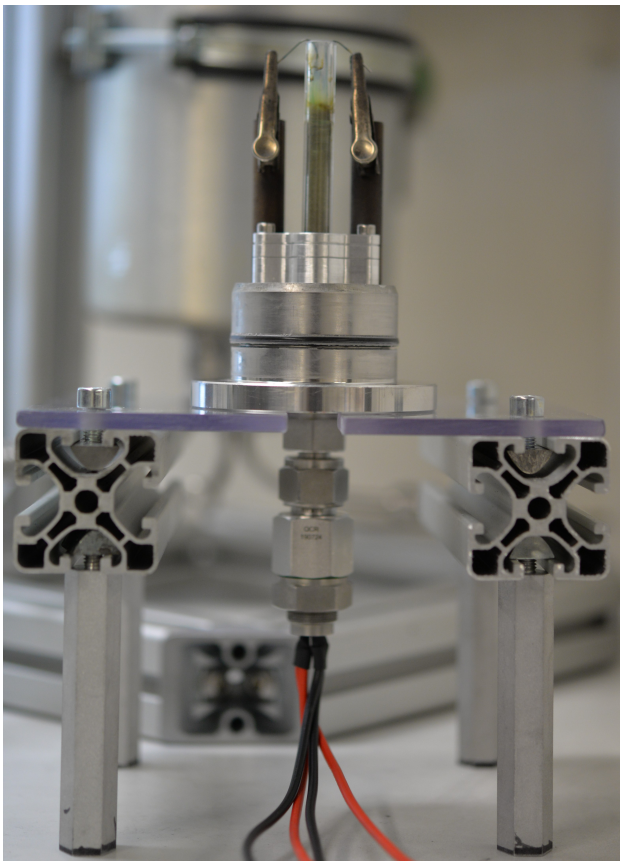

Figure 4.2: Image of the fully assembled strand plug after removal from the combustion chamber following a strand burner test. Glass tube is mounted onto the strand plug with screws and the ignition wire is clamped into the crocodile clips. The cable feedthrough is screwed into the strand plug from the bottom.

with the crocodile clips. Also shown in this image is the COTS pressure tight cable feedthrough used to route the wires for the ignition system into the combustion chamber. Four wires are visible in the image. The reason for this is that, due to the space limitations of the setup, the larger diameter cables required to deliver the high currents to the ignition wire would not fit through the pressure fittings leading to the strand plug. Therefore, instead of two larger diameter wires, four smaller diameter wires were used. This issue would need to be addressed in future redesigns of the setup where higher currents are required.

Once this step is completed the strand plug is inserted into the combustion chamber and fastened with four screws. A view of glass tube inside the chamber is shown in figure 4.3. The design of the strand plug and chamber enabled fast and simple turnarounds between test runs. Alternatively,

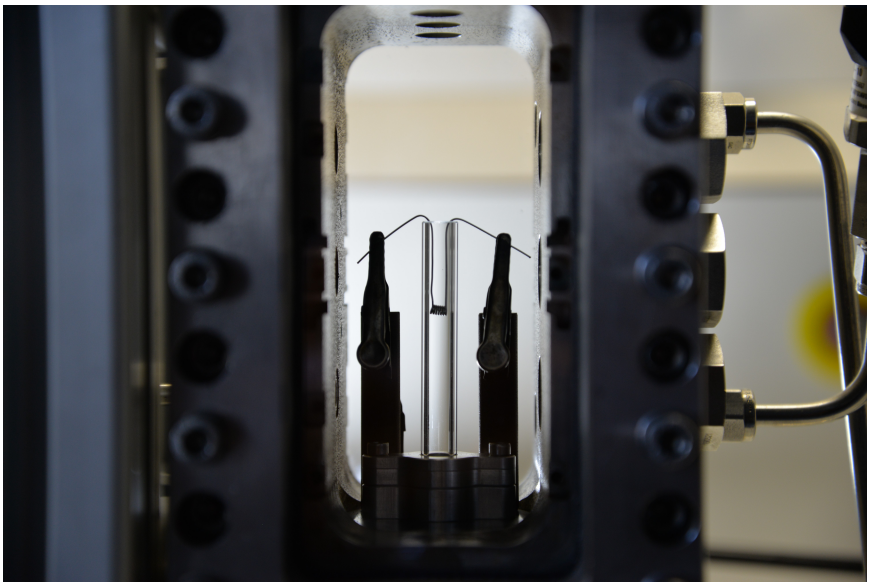

Figure 4.3: Image of the fully assembled strand plug after it has been inserted into the combustion chamber.

access to the chamber could have been possible by removing the window assemblies. This however, would require removing the 16 screws fastening it to the chamber core that would afterwards have to be screwed in again and tightened with the torque required to ensure that the graphite seals could operate correctly. Using an o-ring to seal the strand plug meant that the four screws could simply be tightened with a allen key.

Ignition System

Preparing the ignition system involved adjusting the output settings of the power supply unit. This generally only needed to be done once initially and when changing settings. The power supply unit was equipped with a setting for constant current operation. For this the voltage dial was set to its maximum output and the current turned down to zero. During operation the current could then be increased until the desired value was reached. The voltage would automatically adjust in order to supply the set current. During testing the power supply's current output would always remain the same, regardless of slight differences in wire lengths or other variations, while the voltage would adjust to compensate these differences. As this step could only be done while the power supply unit was operating, a sacrificial wire with a larger diameter was clamped into the crocodile clips and the power supply was activated. This needed to be done before the strand burner was inserted into combustion chamber. The current was set at 12.5 A (13 A in earlier tests) which coincides with temperature between 1100°C and 1400°C according to the wire datasheet [40]. The voltage observed would fluctuate between 7.5 - 8 V. Using equation 3.4 the power can be estimated to between 94 - 100 W. The time until ignition occurred after activation of power supply the varied widely, independent of the pressure, so no estimate for the ignition energy can be provided.

HS Camera

The setup of the HS camera was done within the viewing software (Photron FASTCAM Viewer 4 (PFV4)), provided by the manufacturer. First the resolution is set. For this application a resolution of 128x664 (width x height) is used to limit the recording to only the area of interest, i.e. the glass tube. This setting was saved as a preset for all following tests. Next the frame rate is set. Previous studies reported using frame rates ranging from 500 frames per second (fps) [41] to 1000 fps [42] and even 2000 fps [7, 43, 44]. For the present work a frame rate of 1000 fps were chosen as a starting point. The shutter speed was adjusted for each propellant depending on the brightness of the flame it produced during combustion and varied from 1/2000 s to 1/20000 s. Once these steps are complete the camera is ready to record. As a final step LED panels equipped with light diffusers as backlighting are placed and switched on.

Data Acquisition and Control System

Starting the data acquisition and control system was done by first booting the Raspberry Pi. The control GUI python program is then launched in the terminal. This initializes the microcontroller with input readings and activates output controls and the system is ready for use.

Sample Preparation

The propellants (neat NM and various mixtures) were provided by the DLR. NM required no preparation. The process of preparing the mixtures contains proprietary information that can not be shared within this thesis. Therefore, the mixtures were prepared by a DLR employee.

4.2 Test Execution

In this section the main steps involved in a test run, following the completion of the previously described test preparations, will be described and further key features will be presented.

Once the preparations are complete the test can begin with loading the propellant into the glass tube located in the combustion chamber. This is done by drawing the desired amount - this depended on the where the ignition wire coil should lie in relation to the surface level and was determined during the run-in test - into a syringe equipped with a 120 mm needle. The needle is then inserted into the combustion chamber through the upper access port and into the tube, where the propellant is then injected into said tube. Once complete the access port is sealed using a threaded cap. With the propellant loaded the power supply is turned on but is not yet active. Figure 4.4 shows this point in the testing procedure from inside the laboratory room. The fume hood is illuminated by the LED backlighting showing parts of the fluid system, such as the pressure vessel on the right side of the fume hood, and the combustion chamber. The camera and power supply unit are placed on a table in front of the fume hood. As a final step before leaving the room the valve on gas cylinder containing the pressurant is opened and the desired pressure is set on the pressure regulator valve. The data acquisition and control system is set up in the

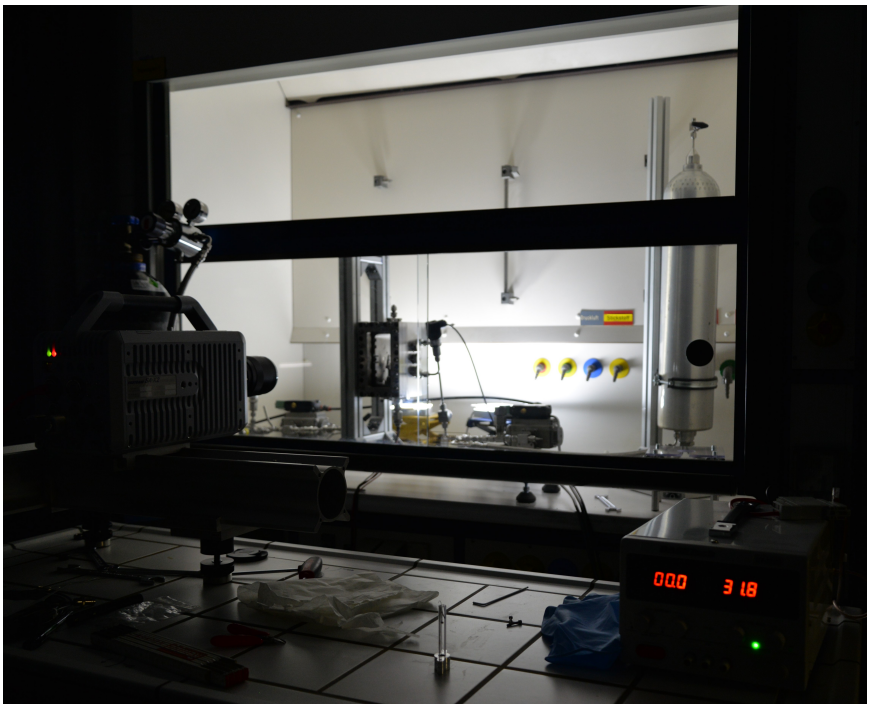

Figure 4.4: The experimental setup from inside the DLR laboratory room just prior to a test run. The combustion chamber and fluid system are placed in the fume hood. HS camera and power supply unit placed on a table in front of the fume hood.

hallway outside of the room and is shown in figure 4.5. It is set up on another table with the PLC located on the lower rack and the monitor, mouse and keyboard and the laptop running PFV4 on the tabletop. After ensuring the outlet valve 2V1 is closed the inlet valve 1V1 is opened using the control GUI and the system is pressurized. Once the pressure stabilizes the valve is closed and the camera is primed for recording in the viewer. The system is armed and the test sequence is initiated. Once the test run is complete the system is depressurized by opening the outlet valve and the HS camera footage is stored. The setup is then reset and prepared for the next test. This involves removing the strand plug and swapping the glass tube.

4.3 Test Plan

The combustion rate tests were divided into to two separate campaigns. First, a run-in test campaign in which only neat NM was tested, served as a method of proving the proper functioning of the experimental setup and to determine issues that required adjustment. Regarding the latter, a focus lay on the ignition method and general testing procedures. Finally, the resulting footage was used to finalize the image analysis tool. The results of this campaign also served as a baseline for comparison with the results of the second campaign. This was an additives test campaign in which the effect of various additives on NM combustion behavior were studied.

Figure 4.5: Experimental setup in the hallway outside the laboratory. The PLC is located on the lower rack and is connected to the monitor, mouse and keyboard on the tabletop. The laptop running the HS camera viewing program is also placed on the here. Red emergency stop button to quickly abort a test run if necessary.

4.3.1 Run-In Campaign

The initial tests were conducted with neat NM as a propellant. This would enable verifying results by comparison with other NM studies conducted in the past. NM ≥98% produced by Carl Roth [45] was used for all tests conducted in the course of the present work.

The experiments were conducted at maximum pressures of 6.0 MPa, as the pressure regimes around 3.5-4.0 MPa and lower are of main interest in the context of NM applications for in-space propulsion systems. The same applied for the following test campaigns. As one of the goals of the combustion rate studies in the present work is to determine the minimum pressure at which combustion can be achieved, and with the previous reports of ignition difficulties at lower pressures, the first tests were conducted at the maximum pressure. The pressure level was then gradually reduced in 0.5 MPa increments until the minimum pressure is reached. At each pressure

level three test runs were conducted, whereby at least two should be successful, this being the case when ignition was achieved and the propellant was mostly or completely burned. Once a potential minimum was reached an additional two tests are conducted to verify that no combustion can be achieved below this pressure level.

4.3.2 Additives Campaign

The mixture were made with the additives presented in section 2.4. The following mixtures were studied in this test campaign:

- 2% iron-based organometallic compound (OMC1) + NM
- 1% OMC1 + NM
- 2% chromium(III) acetylacetonate (CAA) + NM
- 13% organosulfur compound (OSC1) + NM
- 13% OSC1 + 2% OMC1 + NM
- 10% OSC1 + 1% OMC1 + NM
- 6% n-butanol (BUT) + 2% OMC1 + NM
- 6% BUT + 2% CAA + NM

The percentage values for the additives in these mixtures are given in wt.%.
The procedure of this test campaign is analogous to the run-in campaign with the difference that pressure increments are increased to 1.0-1.5 MPa above 3.0 MPa and only two tests were conducted for each pressure level. This was done in order to be able to increase the amount of test series or mixtures that were tested in the course of the present work.

5 Image Analysis Tool

The following chapter will first present an overview of the method used to measure the combustion rate during a strand burner test run. Afterwards, a more detailed explanation for the separate steps involved in the process is given.

5.1 Methodology

As discussed in the previous sections the tests are recorded using a Photron SA-X2 HS camera. To extract the burn rate data from this footage an image analysis tool was implemented in Python using the OpenCV software library which offers a multitude of image processing functions [46]. The complete process of determining the burn rate for a given test is visualized in figure 5.1. The

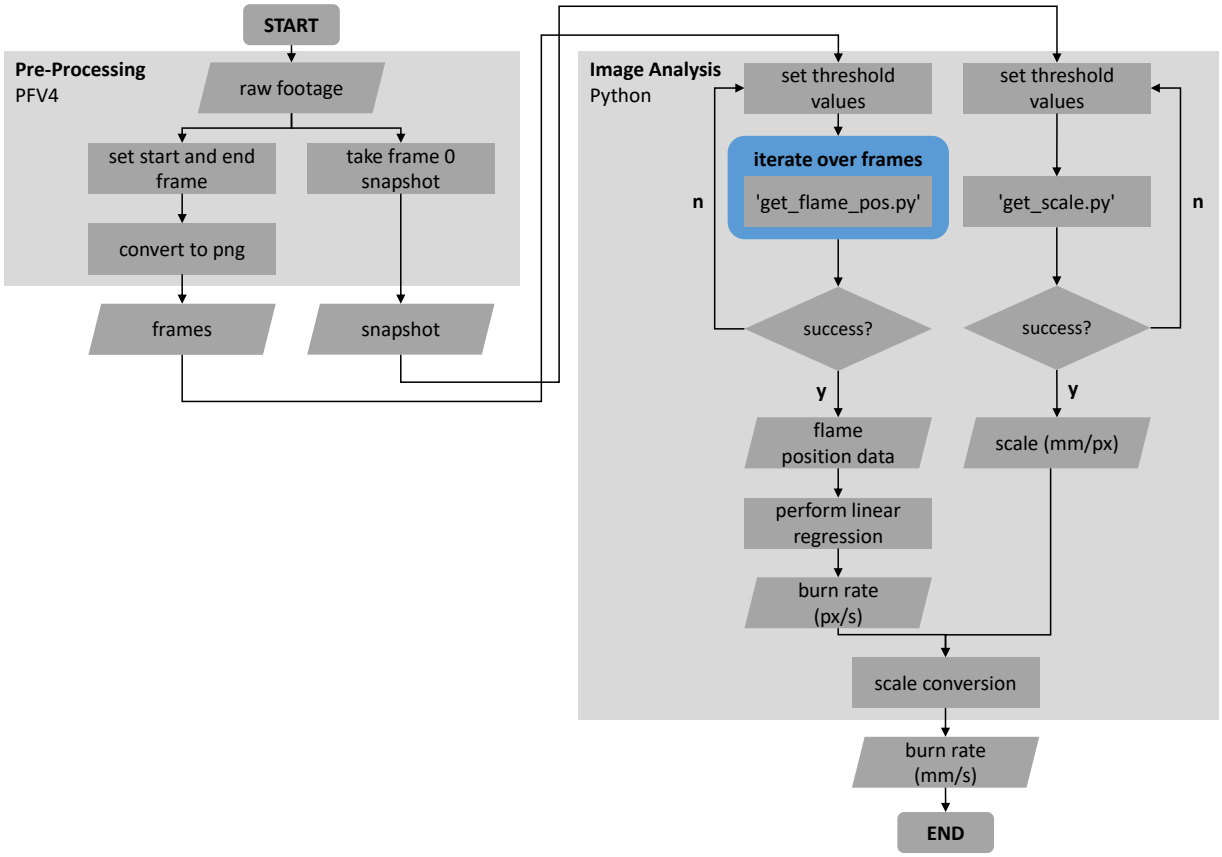

Figure 5.1: Flow chart of the image analysis process starting with the raw HS camera footage as initial input. After running through the pre-processing steps and the implemented image analysis tool the burn rate is extracted from the recorded footage.

process is divided into two stages: an initial pre-processing of the raw HS camera footage and the

subsequent image analysis stage to determine the burn rate. Additionally, the entire process is completed following two separate paths that run through both stages concurrently to determine all the data required, namely, the flame position data and the mm/pixel-scale, to calculate the final output, that is the combustion rate r_b in $\frac{mm}{s}$. The pre-processing is done using the Photron Fastcam Viewer 4, which is the software supplied by the camera manufacturer. To prepare the footage for image analysis it is first converted into images for each separate frame. The starting frame is set after ignition has occurred and stable combustion sets in. The end frame is set to the point where the lower edge of the flame begins to disappear into the tube mount. The chosen frame range is then converted into images with the PNG file format. The start and end frame information is noted to enable synchronization with the recorded chamber pressure data. Finally, a snapshot is taken of the first frame. This will later be used in determining the mm/pixel-scale. The converted frames and snapshots taken serve as the main input for the image analysis step. The tool uses edge detection algorithms for both the tracking of the flame position during a test and for determining the mm/pixel-scale. Threshold values used to calibrate the algorithms are initially set but must be adjusted manually if necessary. Once the respective script is run successfully and produces the desired output a linear regression is performed to determine the burn rate as $\frac{px}{s}$. The mm/pixel-scale is then used to convert this value to the final output of the burn rate in $\frac{mm}{s}$. A more detailed description of the two image analysis functions '*get_flame_pos.py*' and '*get_scale.py*' will be offered in the following sections, beginning with the process of tracking the flame position during a test run.

5.2 Tracking flame position

The objective is to determine the flame position for each frame and track its movement from one frame to the next. The image processing steps that are taken to determine flame position in a single frame are illustrated in figure 5.2. The first step is converting the original image into grayscale. A gaussian blur is then applied to reduce noise. To detect edges the canny edge detection algorithm (CED) offered by the OpenCV library is used [46]. The algorithm detects edges by comparing the intensity of neighboring pixels and finding local intensity gradient maximums. The image is then binarized by suppressing pixels that do not constitute a gradient maximum while the remaining pixels are identified as potential edges. Finally, hysteresis thresholding is applied to decide which of the non-suppressed pixels are really edges and which are not. For this two threshold values are defined, an upper and lower threshold. Pixels with a gradient larger than the upper threshold are considered as a 'sure-edge' while those with a gradient below the lower threshold are discarded as non-edges. Pixels with gradients that lie between both threshold values are classified as an edge if they are connected to a 'sure-edge' pixel (i.e. gradient greater than upper threshold), if not they are discarded as non-edges. The result is a binarized image with the detected edges displayed as thin white curves. The final step is identifying the correct edge that represents the burning surface. To achieve this, contours are drawn into the CED output image. These contours, drawn in red, are derived from those edges that connect to continuous curves. For each contour the lowest point on the curve is determined and of these points, the lowest is again selected and defined as the flame position, marked as a blue dot in figure 5.2. This process is repeated for each

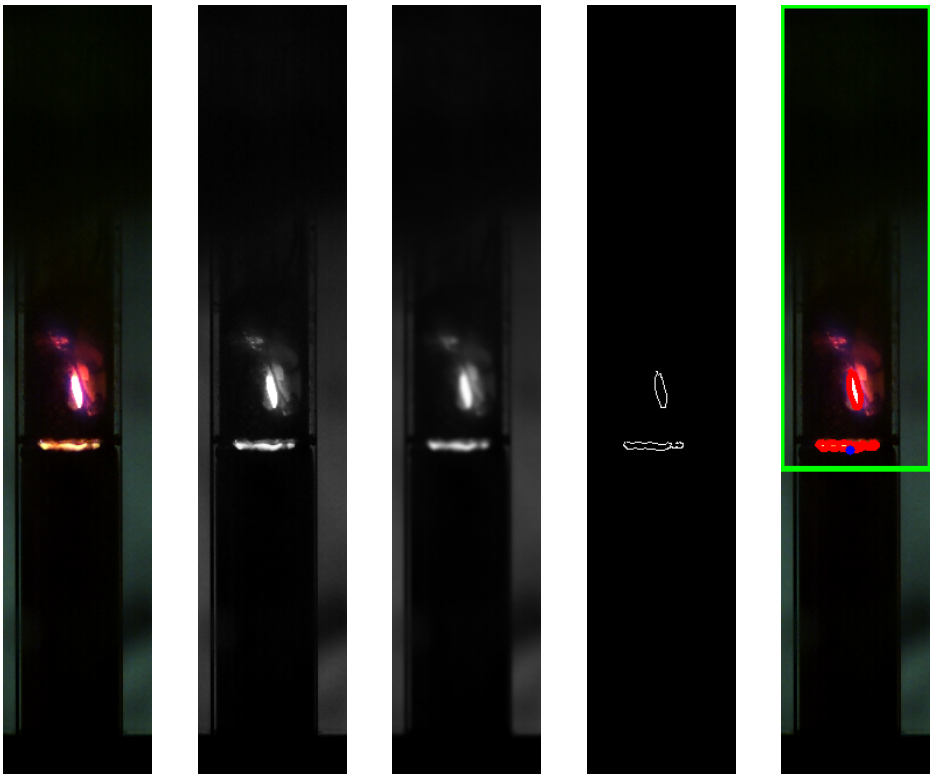

(a) original (b) grayscale (c) blurred (d) CED (e) contours

Figure 5.2: Step by step breakdown of the image processing performed for the flame detection process. (a) shows the original image which is converted into grayscale in (b) as the initial step. In (c) gaussian blur is applied to the image to remove noise. Edges are then detected using the CED algorithm to produce (d). The edges are used to draw contours colored red in (e). The blue dot indicates the lowest point of the lowest contour located within the green boundary box. This point is defined as the flame position.

frame by iterating through the previously set frame range at a set time step. Figure 5.3 shows the tracking of the flame position over multiple frames. Depending on the frames per second (fps) at which the footage was recorded this time step corresponds with a specific spacing between frames for which the flame position is determined. The final output is a list containing the flame positions in pixels for each frame that was processed and therefore the corresponding point in time relative to the initial frame. For this process to produce correct results the burning surface must always be the lowest contour detected during image processing. However, many variables such as recording settings, lighting and reflections, flame brightness, overall image quality and obstruction of view due to exhaust gases have a great influence over which objects and edges are detected by the algorithm. To allow adaptation to changes in these variables two calibration tools were implemented. The first of these are the previously mentioned threshold values used in the edge detection process. They are set high enough such that all irrelevant edges are filtered out but low enough for the burning surface to still be detected. Minimizing the amount of contours detected maximizes the chance that the correct contour is selected. The tool, that was implemented to easily adjust the threshold values, will be presented in a later section. The issue with this method

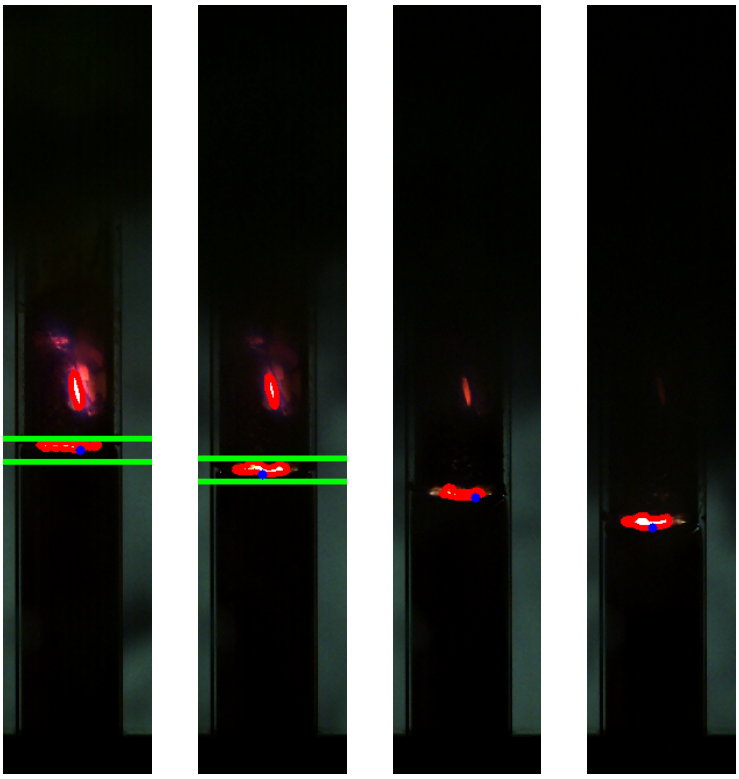

(a) T +0.0s. (b) T +2.5s. (c) T +5.0s. (d) T +7.5s.

Figure 5.3: Tracking flame position over multiple frames. A time step of 0.1s (100 frames) was used to produce these images. To better illustrate the movement of the flame a time interval of 2.5s between these example images was used. The red contour indicates the edges detected by the CED algorithm. The blue dot indicates the flame position. The green boundary box is only necessary when multiple contours are detected as seen in images (a) and (b).

is that one set of threshold values that may work for one frame, may produce an undesirable result for the next frame where a new edge may appear due to numerous reasons that is falsely identified as the burning surface. To ensure in this case that the correct contour is selected, a heuristic method is used. A boundary box (see green boxes in figures 5.2 and 5.3) is created around the previous flame position. A contour can only be identified as the flame if it lies within this boundary box. If none of the detected contours qualifies the threshold settings must be adjusted. This is also the procedure if no contours are detected, which would indicate that the threshold values are too high. The size of the boundary box itself can also be adjusted. This is especially relevant for the first frame being processed, as there is no previous frame and corresponding flame position around which the boundary box can be drawn. Therefore it is drawn to the top, left and right borders of the image and the lower edge of the box is set just below where the initial burning surface is expected to be.

The flame position data is then used to determine the combustion rate as $\frac{px}{s}$ by performing a linear regression as shown in figure 5.4. It shows the flame position over time determined with the previously described process. The default cartesian coordinate system by which pixel positions are defined has its origin in the top left corner of an image. The y-axis corresponds to the height,

therefore an increase in the y-axis direction corresponds to a movement downwards. Using these

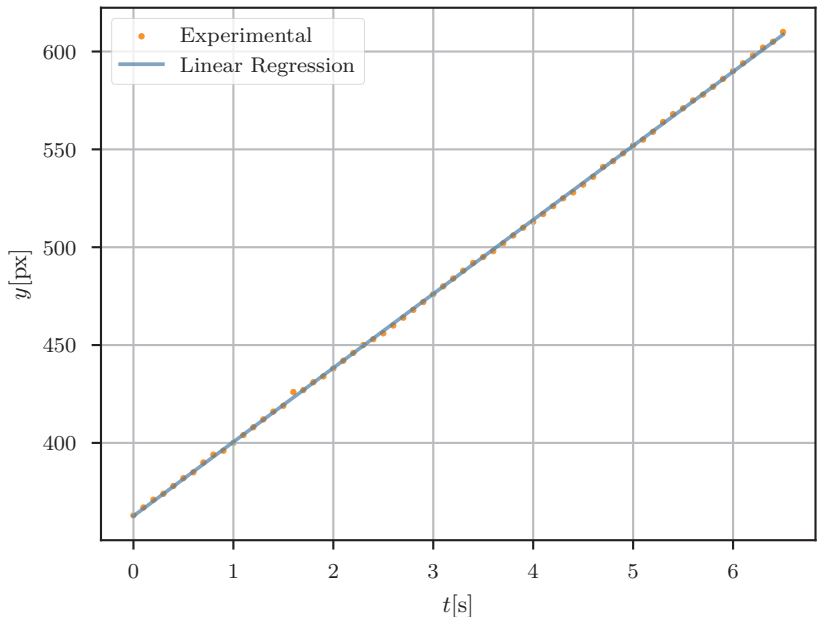

Figure 5.4

data points a linear least-squares regression delivers the slope and y-intercept of the plotted linear function. The slope of the resulting function corresponds to the combustion rate.

5.3 Determining scale

In order to convert the burn rate determined using the '*get_flame_pos.py*' function from $\frac{px}{s}$ to $\frac{mm}{s}$ the dimensions of a pixel in mm must be determined. To do this a known distance is measured via image processing. Since the diameter of the borosilicate tube is known and its position inherently coincides with that of the flame, it is ideally suited for this purpose. An additional advantage in using the tube for the scale determination is that changes in the positioning and orientation of the camera relative to the chamber between tests - due to bumping against the camera or the table on which the camera is positioned - does not influence the accuracy of the measurement. This stems from the fact that the process is performed for each separate test run using the snapshots mentioned in the beginning of this section. These snapshots are created using the same raw footage used for the flame tracking.

The image processing steps taken to determine the mm/pixel-scale are shown in figure 5.5. This process again uses CED to detect edges. However, no gaussian blur is applied after the conversion to grayscale. This is due to the nature of the snapshots used. They are taken from the first frame of the recording where no additional source of light (flame or glowing wire) is present. Therefore, the intensity gradients are much lower throughout the entire image and adding blur to the image on which the edge detection algorithm is used may make the tube edges to difficult or impossible

to detect. After identifying the edges in the image a hough line transform (HLT) is used to find

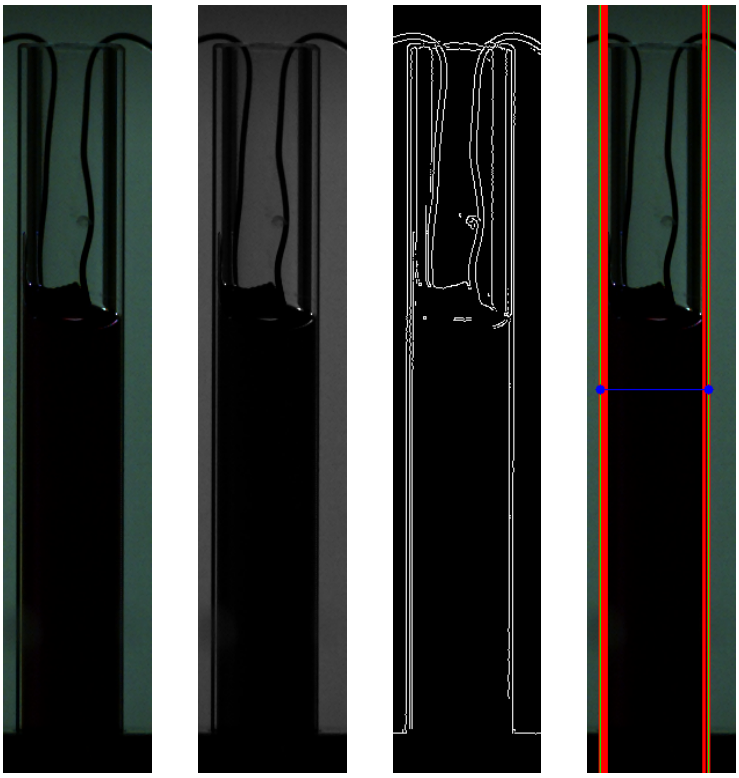

(a) original (b) grayscale (c) CED (d) HLT

Figure 5.5: Steps to determine scale using canny edge detection and hough line transform to find edges of tube. (a) shows the original image. In (b) it is converted to grayscale.(c) shows the result of the canny edge detection algorithm (CED). The detected edges are used to find the edges that form straight lines using a hough line transform (HLT) in (d). Of these lines colored in red the outermost lines (green) are selected as the tube edges and the distance between them is calculated and drawn into the image in blue.

those edges that combine to form straight lines indicating that these edges coincide with the edges of the tube. The HLT works by finding all edge points which are located on the same line. If the number of points on a given line exceeds a set threshold value it is declared as a line in polar coordinates [46]. As the tube edges are inevitably the longest straight, near vertical lines in the image - apart from the image borders - the HLT threshold value is set high enough to remove all of the lines with only a few points located on them (e.g. ignition wire). These lines are then filtered by angle, removing all lines with greater than 1°deviation from the vertical axis. Since light is reflected on both the inner and outer surface of the tube walls, there still remain multiple lines from which the correct tube edges must be extracted. This is easily done by selecting those lines that are closest to the left and right image borders. For the sake of simplicity, parallelism of the two lines is not a requirement for selecting these lines as the tube edges. As a result, the distance between the lines may vary depending on the height at which the distance is measured. In order to minimize the effect of these variations this height is set to half the height of the tube. With the

known tube diameter of d_{tube} and the measured distance d the mm/pixel-scale sc is calculated as shown in equation 5.1.

$$sc = \frac{d_{tube}}{d} \tag{5.1}$$

This scale can then be used to convert pixel values to mm values. In the case of the burn rate calculated from the flame position data this is done as shown in the following equation 5.2.

$$r_{b,mm} = r_{b,px} \cdot sc \tag{5.2}$$

5.4 Calibration

If during the image analysis process either of the two scripts is not executed successfully, its threshold values need to be adjusted. In the case of '*get_flame_pos.py*' this happens if no contours are found, no contours are found within the boundary box or the incorrect contours are determined as the burning surface, resulting in an incorrect flame position being selected. For the '*get_scale.py*' function the process is deemed unsuccessful when no or only one line was detected. For both the flame position tracking and the scale determination a calibration script was implemented in order to easily adjust the threshold values. Figure 5.6 shows a demonstration of the calibration script for the flame position tracking process. Starting the calibration script opens three windows: the CED output, the drawn contours (red) including the selected flame position (blue) and a window containing trackbars that enable the user to change the threshold values. On the left side of the figure the initial threshold values are shown with the result of the flame position detection process displayed underneath. As only single frames are being examined, the boundary box serves no purpose here and has been expanded to the image borders. In this example the threshold values have been set too low, which leads to an incorrect flame position being selected in the bottom most contour. This contour is a result of the tube edges being detected by the CED. The goal is now to raise both threshold values until all or most unwanted contours are filtered out and the flame position is selected correctly. While changing these values using the trackbars the outputs are updated in real time making this process fast and simple. The results are shown on the right side of the figure. The only remaining contour is the actual burning surface. The threshold values can now be transferred to the flame position tracking script and the script can be rerun.

The procedure for the scale determination process is analogous to the one previously described, with the minor difference that two additional trackbars allow the user to change the HLT and angle threshold values.

5.5 Measurement Uncertainty

As the implemented tool is custom in nature, no precedent exists from which estimation of measurement uncertainty can drawn. Therefore, an attempt was made to first identify and then quantify the measurement errors associated with this method of combustion rate measurement. The exception to this is the measurement error of the pressure sensor used, which can be taken

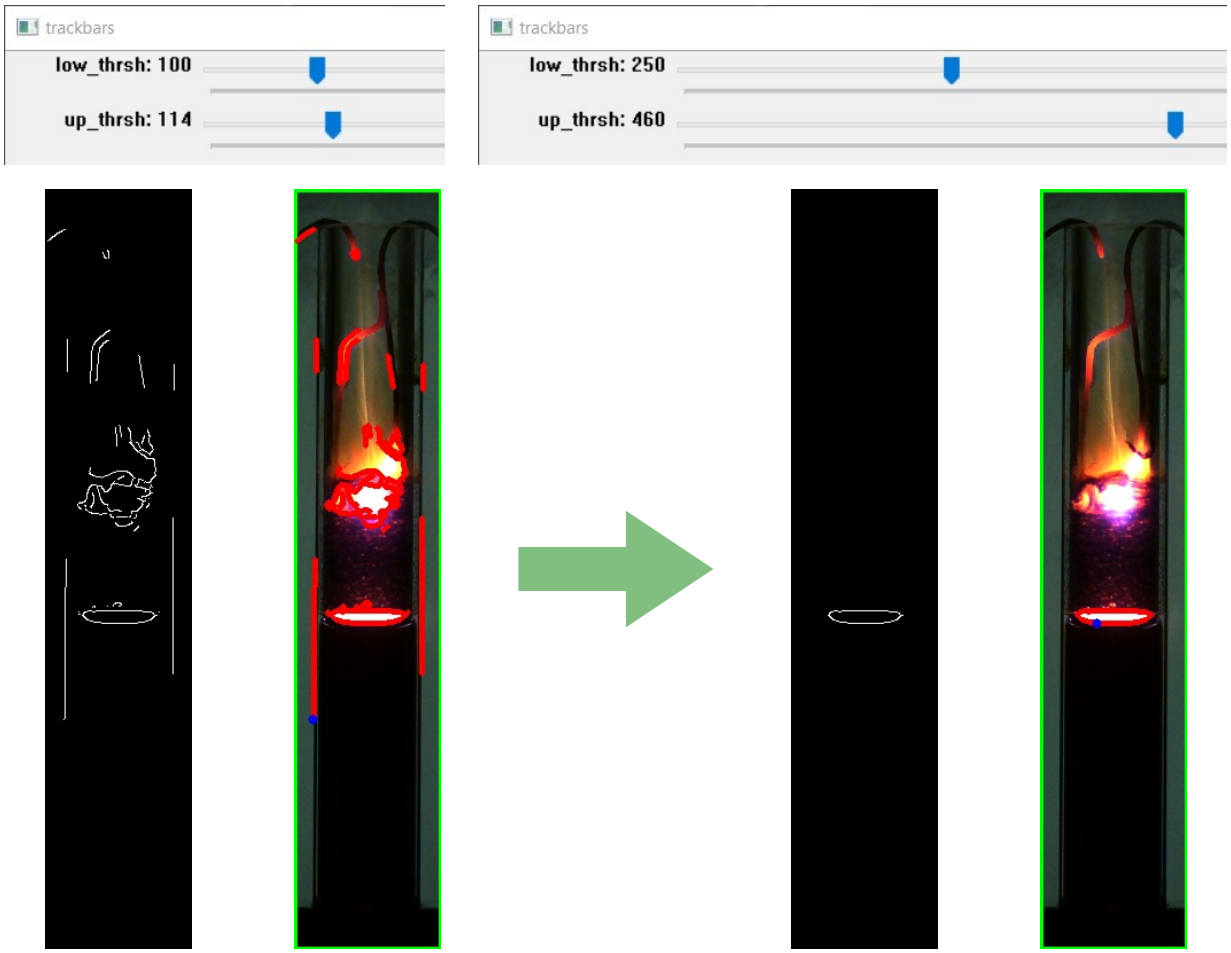

Figure 5.6: Demonstration of the calibration process for the flame position determination script. Initial threshold values on the left used for edge detection result in incorrect flame position selection (blue dot). After adjustment of the values using the trackbars, unwanted edges are filtered out and correct flame position is detected.

from the datasheet [35]. The measurement error accrued from the scale determination is split into three separate error sources.

- flame tracking: an error range of ±2 pixels was used for flame position determination. This error was applied to the slope derived from the flame position over time data.
- scale determination 1: as the mm/pixel-scale is derived from the tube diameter, the dimension tolerance of ±0.15 mm is used.
- scale determination 2: an error range of ±2 pixels is used to account for incorrect tube edge detection.
- scale determination 3: as edge selection is simplified by selecting the outermost lines detected by the HLT without an additional check if these lines are parallel, an angle error is accrued based on the angle threshold. This value was set to 1°. Assuming both selected lines are

slanted away from each other at the maximum angle an additional maximum error along the length of the lines (image height of 664 px) of ±10 px is used.

- pressure: an error range of ±0.1 MPa was used for pressure measurements (taken from the pressure sensor datasheet [35].

6 Results and Discussion

In this chapter the experimental setup that was developed within the present work is reviewed on the basis of the requirements defined in chapter 3. Next the results and findings of the strand burner tests are presented and discussed, beginning with the overall results and following up with a closer look into the separate propellant mixtures that were tested. Additionally, difficulties and problems that were encountered during testing and the subsequent evaluation with the image analysis tool will be addressed.

6.1 Experimental Setup

The strand burner test stand was designed based on the requirements defined in table 3.1. In the following it will be discussed to what extent these requirements were met, and if not, the reasons for this will be elaborated.

Beginning with the functional requirements the functions defined in requirement F.1 were, for the most part, demonstrated during the test campaigns. This included the holding, igniting a burning of a liquid propellant, that was being held in a container (glass tube), in the fashion described by this requirement. Viscous or gelled propellants were not tested within the present work and could therefore not be demonstrated, but it can be reasonably assumed that the setup is capable of functioning as required for these types of propellants. F.2 was equally demonstrated and was therefore fully met. The combustion chamber equipped with opposing viewing windows and the use of transparent glass tubes as the container for the propellant enabled the optical access demanded by F.3. Finally F.4 was fulfilled by use of a HS-camera to record test footage and an image analysis tool to obtain the combustion rates from the recorded footage. However, it must be mentioned that, as it was not possible to generate results for neat NM combustion rates by which a comparison with results from other combustion rate studies would be enabled (see section 6.2), the measurement method could not be verified. Nevertheless results from the subsequent additives test campaign do mirror behavior observed in a previous study by Ziemer [27] and can therefore be reasonably assumed as valid and this requirement is deemed to be at least partially fulfilled.
The first design requirement D.1 was only partially fulfilled as all of the attempted methods to characterize the chosen ignition method were unsuccessful. Instead the ignition wire specifications provided by the manufacturer together with the observed power supply output were used in order to estimate wire temperatures during ignition. Safe operation of the experimental setup was guaranteed by the use of redundant safety features implemented in the fluid system (relief valve, burst disc) and through remote operation enabled by the control system. Therefore, requirement D.2 is also deemed as fulfilled. Table 6.1 summarizes the review of the requirements for the experimental setup.

Table 6.1: Review of the requirements defined in section 3.1. '**Y**' denotes if a requirement is fulfilled, '**N**' if it is not. '**P**' denotes if a requirement was partially fulfilled.

ID	Description	Fulfilled
F.1	The setup shall be able to hold, ignite and burn a liquid, viscous or gelled propellant strand or column, i.e. a volume of propellant held in a container in such a way that it can be ignited on one end (top) and burn to the other end (bottom).	**Y**
F.2	The setup shall enable ignition and combustion in a chemically inert atmosphere at constant pressures up to 6.0 MPa by means of a pressure vessel.	**Y**
F.3	The setup shall allow optical access to the propellant strand or column meaning both the container and the pressure vessel shall allow optical observation of the ignition and combustion processes.	**Y**
F.4	The setup shall enable the measurement of the propellant combustion rate.	**P**
D.1	The means of ignition shall be characterized with a variable and well-defined ignition temperature or energy.	**P**
D.2	At no point during preparation, execution or follow up of the experiments shall the user or observers be exposed to any risk of harm.	**Y**

6.2 Combustion Rate Studies

As described in chapter 4 experiments were initially divided into two test campaigns: a run-in test campaign, in which the proper functioning of the setup was checked and verified using neat NM, and an additives test campaign to test the previously introduced additives (see chapter 2) separately or in combination with one another. HS camera footage of the run-in campaign was also used to test and finalize the image analysis software in preparation for the remaining tests.

Table 6.2 offers an overview of the scope of experiments carried out in the course of this work. In total, 160 tests were conducted of which 123 were considered successful, meaning that the propellant ignited and burned mostly or completely. For initial tests conducted with the higher concentration OMC1 mixture and CAA mixture, three tests were performed at every pressure level starting at 5.5 - 6 MPa and lowering the pressure in 0.5 MPa increments until the minimum pressure at which sustained combustion occurred was reached. For all following test series, the amount of test runs per pressure level was reduced to two and the pressure between increments was increased at pressures above 3.5 MPa to allow faster completion of the test campaign. In the case of neat NM it must be noted that no sustained combustion could be achieved with the selected ignition method. Due to the modified method of ignition used in these tests the results can not be considered representative for the use case being investigated within this thesis (i.e. use as monopropellant). This will be explained in more detail in section 6.2.1. The combustion rate for each test was determined using the HS camera footage and the image analysis software introduced in chapter 5. These values were then used to find the coefficients for the empirical

Table 6.2: Overview of all tests conducted as part of the initial run-in and subsequent additives test campaign with the number of attempts and the number of successful tests. A test was deemed successful when the propellant ignited and burned mostly or completely. *invalid due to method of ignition.

Mixture	No. tests	No. successful tests
Run-in campaign		
neat NM	*14	6
Additives campaign		
2OMC1	33	29
1OMC1	13	10
2CAA	33	23
13DS	16	11
13DS2OMC1	15	14
13DS2CAA	9	8
10DS1OMC1	15	12
6BU2OMC1	12	10
6BU2CAA	4	0
total	164	123

power law equation 2.7 introduced in section 2.1.2 using a regression analysis.
In the following sections first the neat NM tests are presented and discussed. After plots of selected propellant mixtures are be presented and discussed in more detail. The mixtures are divided according to the type of additive used. First, those containing only catalysts are be presented to show the effect they have on the combustion rate compared to neat NM. Next, those mixtures containing inhibitors are presented. As these were generally used only in combination with a catalyst these mixtures will be further divided according to the catalyst additive. As mentioned previously no usable results for neat NM could be generated. Therefore, values from similar setups from Boyer and Kuo [7] and McCown et al. [8] are used as a baseline reference.

6.2.1 Neat Nitromethane

No sustained combustion could be achieved in neat nitromethane tests using the standard ignition method. However, during testing, other methods were tried of which one resulted in successful ignition and sustained combustion.
Figure 6.1 shows several frames from different stages of one of these tests. To achieve the result the wire was lowered into the tube so that a significant portion of the propellant was above the coil. When the power supply was turned on at T -0 s the wire began to heat the surrounding fluid, acting similarly to an immersion heater. Vaporization of the fluid at the coil and around the wire leads in the propellant column above could be observed, so it can be reasonably assumed that these areas were heated to around the boiling temperature of NM at 5.4 MPa with the remaining fluid also experiencing an increase in temperature. The part of the wire that was not submerged

was able to heat up to above 1100°C (taken from the datasheet for a current of 13 A [40]) and after a short while ignited the propellant vapors. The flame progressed down the tube in turn heating the wire above its melting temperature at 1400°C at which point the wire broke on one side, thus cutting off the current.
The flame would extinguish itself when it reached the coil or in some cases shortly after passing the coil. This coincides with the volume of fluid that was heated to the boiling temperature so it can be assumed, that the 'preheating' done by the wire before ignition was the main reason why combustion could be sustained. Therefore, sustained combustion was not achieved independently but only under the influence of the heat generated by the ignition wire.

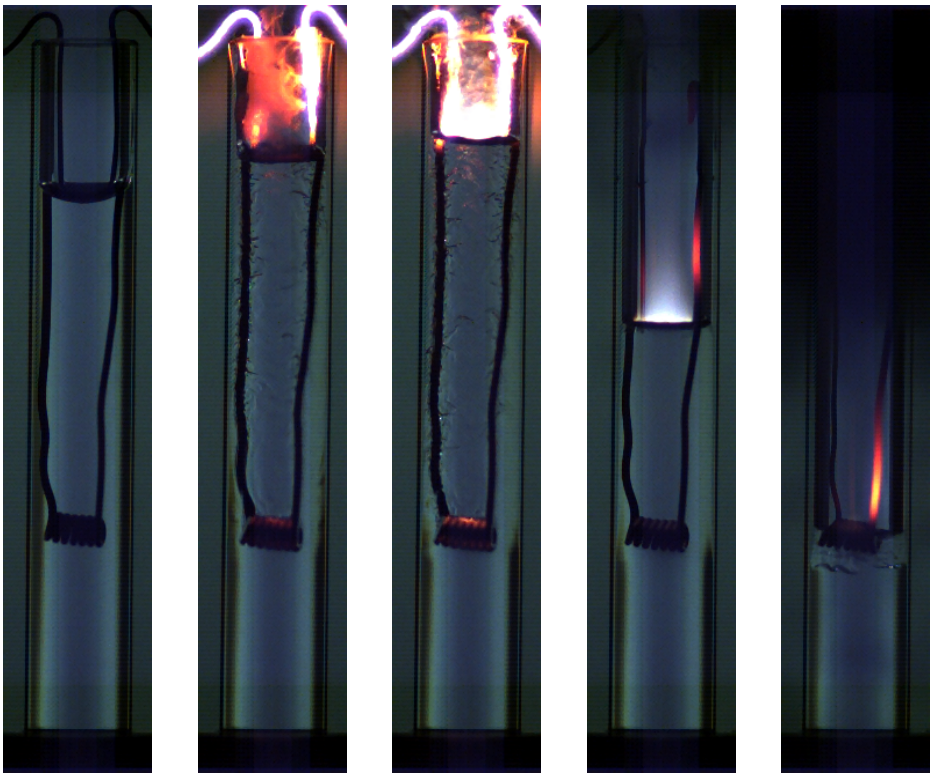

(a) T -0 s (b) T +3 s (c) T +4.2 s (d) T +10 s (e) T +20 s

Figure 6.1: Frames from a neat NM test at 5.5MPa using the 'preheater' ignition method with 13A of current. (a) Power supply is turned on. (b) Wire reaches equilibrium temperature above 1000°C. (c) Ignition. (d) Stable combustion. (e) Flame extinguishes itself.

This influence is better illustrated when looking at the flame position over time plot in figure 6.2. The combustion rate at any point in time equates to the slope of the curve at that specific point in time. As the curve is convex, the burn rate must be decreasing while the flame progresses further downward. Since the wire breaks shortly after ignition, (this is indicated by the state of the propellant column above the coil: in image 6.1c vapor bubbles are visible and the wire is glowing hot while in the next image 6.1d the fluid is still and the wire is being heated only by the flame, hence the slight glow right above the surface), no further energy is being supplied to the reaction and the burning rate begins to decrease. But the fluid column above the coil has already been preheated, so that the effects of this preheating only slowly decrease as the fluid cools.

A linear regression was performed to determine the linear function plotted in figure 6.2. After conversion to mm from pixels this delivers a combustion rate of $r_{b,NM} = 2.03\frac{mm}{s}$ at 5.4 MPa. Compared to the reference values from McCown et al. [8] in table 6.3 at this pressure level, with a value of $r_{b,NMref} = 1.29\frac{mm}{s}$ at the given pressure, this value is significantly greater. As other reference values from previous studies do not differ from one another to this degree (see table 2.3), it can be reasonably assumed that this difference is in some way connected to the ignition method.

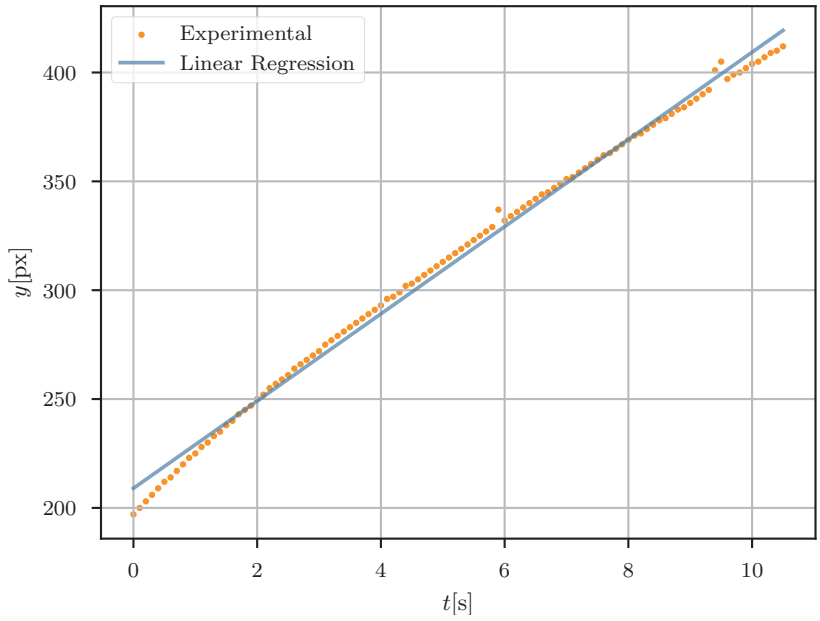

Figure 6.2: Results of image analysis software to determine burn rate of a neat NM strand burner test at 5.4MPa. Linear regression was performed to calculate linear burn rate from flame positions detected in each frame.

Since burning the propellant in this way is not representative for its use as a monopropellant, these tests were deemed unsuccessful in the context of this thesis. However, it might be interesting to study why this method produced these results (a greatly increased burn rate compared to other studies) and to determine whether this is only the result of the preheating, since according to [12], higher temperatures increase reaction speeds, or if the wire material (NiCr) may have some catalytic effect on the reaction, much like other materials for ionic liquids [3] or stainless steel for NM [12, 8]. Furthermore, since these tests were not continued, the lowest pressure tested was 5 MPa. It would be interesting to see if this method can extend pressure ranges below those that were determined in previous studies, where the lowest pressures at which combustion could be sustained were around 3.5 MPa [7, 8].

Other variations of the ignition wire method, which were presented in chapter 3, were also attempted. The method which involved wrapping the wire around the tip of the tube, which had been applied with success in previous studies, reportedly achieving ignition and sustained combustion at pressures where other methods required the aid of solid booster pellets, did not perform as

expected. Propellant at the tip of the tube would boil off without igniting until its surface level had passed the coiled wire or until the wire broke and interrupted the current. If the wire broke after this point the generated heat was not sufficient to continue boiling the propellant and the test was aborted. An explanation as to why this method may not have worked is the difference in the setup Fuller et al. [36] used compared to this work. For one, the successful low pressure test was conducted at 2.9 MPa in air. Due to the presence of oxygen in the atmosphere, it must therefore be considered a burn as a bi-propellant. Next, the setup was a continuous flow strand burner, meaning that the propellant was continuously fed into a quartz glass tube. This ensured that the reaction zone was located within the wrapped section of the tube at all times. An assumption could be made that some preheating of the propellant occurs before reaching the tip of the tube. This would support the hypothesis proposed above. However, no values for combustion rates were supplied in the study. Due to the nature of the method, requiring sustained operation and the ability to re-ignite without having to replace the wire, a larger wire was used with a diameter of 0.65 mm compared to 0.51 mm used in the present work. The smaller wire was not suited for this application, since in most cases the wire broke shortly after the propellant began to boil. Finally a quartz tube with a smaller outer diameter of 6.4 mm was used and - though it was not specified - it can be assumed that the inner diameter in turn was also smaller than the 6 mm used in this work. Contradictory to the assumption this may have had an effect different studies by Derk [14] and Sabourin et al. [17] both concluded that tube diameter has no effect on combustion behavior of pure NM.

6.2.2 Catalysts

Figure 6.3 shows the results of the regression analysis for the combustion rates of the propellant mixtures containing catalyst additives. Error bars illustrate the error resulting from the combustion rate measurement errors (y-axis error) determined in chapter 3. The x-axis error resulting from the pressure measurement error is not shown as it is negligible at ± 0.1 MPa (see section 5.5). The y-axis error stems from the error in determining the flame position in each frame, and the scale that was determined in order to convert the values from pixels to mm during image analysis. As expected, both catalysts OMC1 and CAA increased the overall combustion rate in comparison to neat NM. Additionally, both additives reduced the minimum pressure at which NM burns with OMC1 producing the best results for both characteristics. Notably, only the addition of a catalyst allowed the ignition and subsequent independent (i.e. without the aid of additional energy being supplied to the reaction through the wire) decomposition and combustion of NM in this setup. Both additives extended the pressure range to lower pressures with CAA burning at pressures as low as 2.5 MPa and OMC1 at 1.75 MPa at lower and 1.5 MPa at higher concentrations. Both additives also influenced the shape of the combustion rate curve. For mixtures containing OMC1 a reduction of the gradient with increasing pressures and can be observed, making it a degressive correlation and reducing pressure sensitivity of the combustion rate with a pressure exponent of $n < 1$. This effect was amplified with increasing concentration. CAA on the other hand amplifies neat NMs progressive nature and enhances its pressure sensitivity.

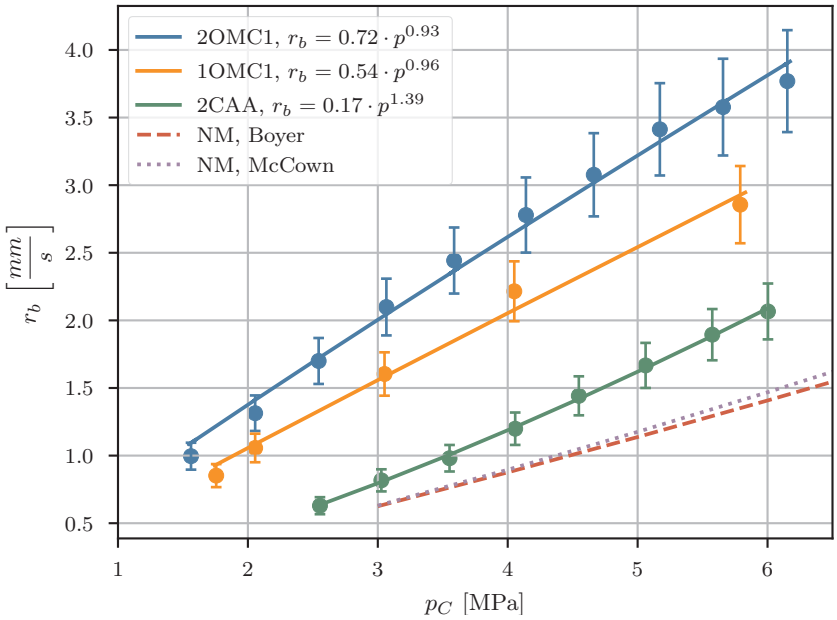

Figure 6.3: Combustion rates for of mixtures of NM and catalyst additives. For each pressure level at which tests were conducted the mean values for r_b and p were calculated. Error bars indicate the estimated error for the combustion rate measurements. The combustion rate for pure NM from previous studies was added to serve as a baseline reference.

OMC1

Of the 46 OMC1 tests conducted in total, 33 were performed with the higher concentration OMC1 mixture with 29 successful tests and 13 where later performed with the lower concentration mixture with 10 successful tests (see table 6.2).
The ignition method (whereby a coiled wire is dipped into the propellant), which was introduced in section 3.2.3, was successfully applied for all of these tests, though some slight adjustments were made that will be further elaborated on below.

Since the actual run-in test campaign with neat NM was not continued, the initial catalyst additive tests can be considered as additional run-in tests, during which minor problems were identified and adjustments were made when necessary. Figure 6.4 shows different stages of a test conducted at 1.5 MPa with the higher concentration OMC1 mixture, starting at T +1.5 s after the power supply was turned on. Similar to the previously described NM test (see 6.1), the unsubmerged part of the wire heats up to above 1100°C (taken from the datasheet for a current of 12.5 A [40]) in figure 6.4a before the vapors ignited in 6.4b. Shortly after this the wire breaks on one side, however, this can not be observed due to exhaust gases blocking the view. In figures 6.4b and 6.4b the flame burns downwards before it reaches the bottom at 6.4e. Apart from the exhaust gases obscuring the view, solid exhaust products, such as soot, are deposited on the inner tube wall so that most of the flame is not visible.
First tests showed that the brightness of the flame required an increase of shutter speed while

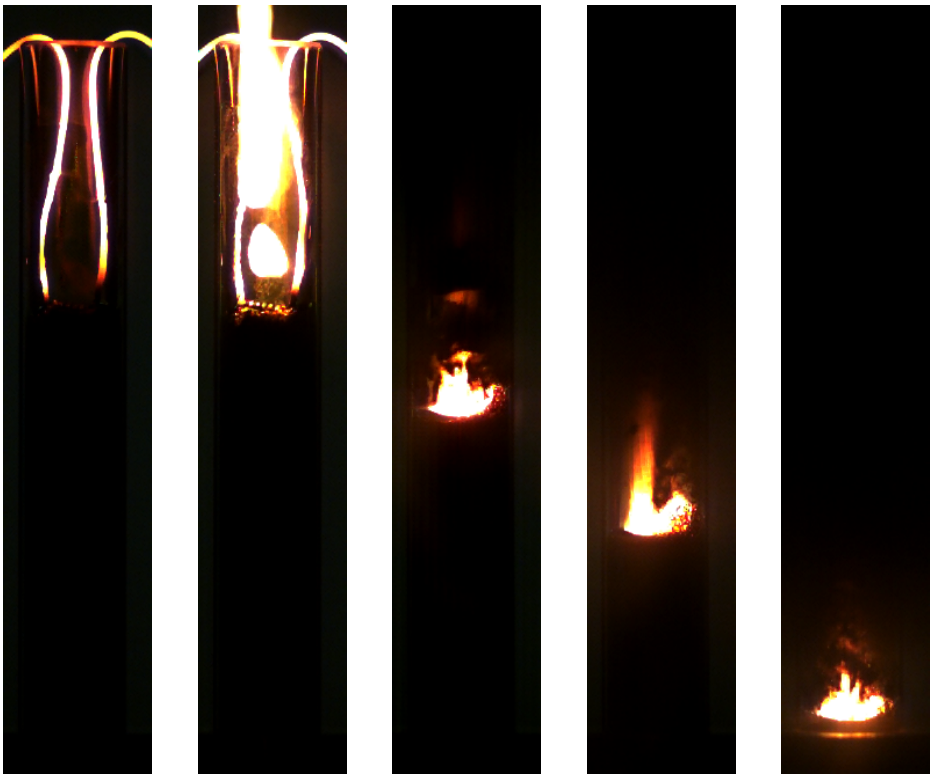

(a) T +1.5 s (b) T +1.9 s (c) T +10 s (d) T +20 s (e) T +36 s

Figure 6.4: Frames from a OMC1 test at 1.5MPa using the standard ignition method with 12.5 A of current. (a) Wire reaches equilibrium temperature above 1000°C. (b) Ignition. (c)-(d) Stable combustion. (e) Flame reaches bottom of tube.

recording in comparison to the neat NM tests, making the recording substantially darker, but preventing overexposure of the camera sensor. Furthermore, it was shown that the production of smoke or vapor in the chamber was a major issue regarding the visibility of the flame. This issue was addressed by lowering the wire further into the tube so that it was hanging 2.5 cm from the top. This allowed the flame to reach the bottom before the exhaust gases could block the view. However, in some cases at lower pressures and subsequently lower burning rates, exhaust gases could partially obscure vision towards the end of the test. The amount of propellant used in each test was chosen so that the wire coil was at least half way submerged but never deeper than about 1-2 mm below the surface. Any deeper would increase the ignition delay, as the wire would take longer to heat up. This resulted in roughly 1.4 ml of propellant being used for each test. The single failed test that was not due to user error or testing below the minimum required pressure for combustion occurred when both ends of the wire broke and the glowing hot coil fell into the tube, almost instantly vaporizing, igniting and burning the remaining propellant. This rarely happened but seemed to coincide with tests where ignition delay was high. If the time until ignition is high the part of the wire not submerged has more time to heat up more evenly, rather than one hot spot forming on one of the leads. At ignition, chances are then higher that both ends of the wire reach their melting temperatures and break at the same time, allowing the coil to

fall into the tube. Additionally, at this point the coil is no longer submerged and has also reached temperatures above 1100°C and it therefore ignites the propellant on contact.

For some of the tests the power supply voltage was observed. This was done visually as no recording of the power supply output was implemented as part the data acquisition system. When set at 12.5 A voltage would rise from about 6.5 V when the power supply was activated, to 7.5 - 8 V and remained steady until ignition. After ignition Voltage would increase to a peak of 9.5 V before dropping to zero after the wire broke. When set at 11.5 A voltage was marginally lower but behavior remained the same. The rise in voltage after ignition can be explained by the wire materials (NiCr) positive temperature coefficient of resistance [40]. Having a positive temperature coefficient means that resistance increases when temperature increases. So when the propellant ignites and heats the wire further it raises its resistance and the power supply must increase the voltage to maintain the set current.

Chromium(III) acetylacetonate

A total 33 tests were conducted with the mixture containing CAA as propellant of which 23 where deemed successful. This high failure rate was not a result of propellant performance, but of issues regarding the setup and human error (such as a clogged filter effecting pressure readings or pressure data being overwritten accidentally), testing below the minimum required pressure for combustion or the previously described scenario in which the hot wire drops into the tube. This occurred four times during this test series. Two attempts were made to ignite the mixture in which the wire was not in contact with the propellant, instead it was hanging just above the surface. However, in both cases the wire broke before ignition was achieved. An explanation for this could be that the wire reached its melting point at 1400°C solely due to the electrical current passing through it, as no flame contributed in heating the wire additionally. However, the current was set to 12.5 A for every test in this series which, according to the wire manufacturer, should heat the wire to a temperature slightly below the operating temperature of 1150°C and well below the wires melting temperature. This would suggest that either the information supplied by the wire manufacturer is not accurate, or that some process is taking place that leads to the increased wire temperature. This only occurred when the wire was not submerged. Having the wire dip into the propellant may let the fluid act as a heat sink letting the wire remain below its melting point and giving propellant more time to ignite before the wire breaks. As these tests were some of the first attempts, this method was chosen for all remaining test series of the additives campaign.

Figure 6.5 shows the stages of a CAA test starting at T-0 s. The pressure was set to 5 MPa and power supply output current was set to 12.5 A. Since the flame of this mixture was less bright, shutter speed could be reduced from that used for OMC1 tests, so that the placement of the wire and how far the wire is submerged is visible in frame 6.5a. As mentioned above, positioning the wire coil this way, in relation to the propellant surface, proved to be successful and was applied in all of the remaining tests. The following stages are similar to those previously described in the OMC1 tests. Since overall burning rates for CAA were significantly lower, obstruction of view due to exhaust gases was more of an issue compared to OMC1 tests. This can be seen in frames 6.5d to 6.5f, although at this pressure the burning rate was high enough for it not to be an issue. Next,

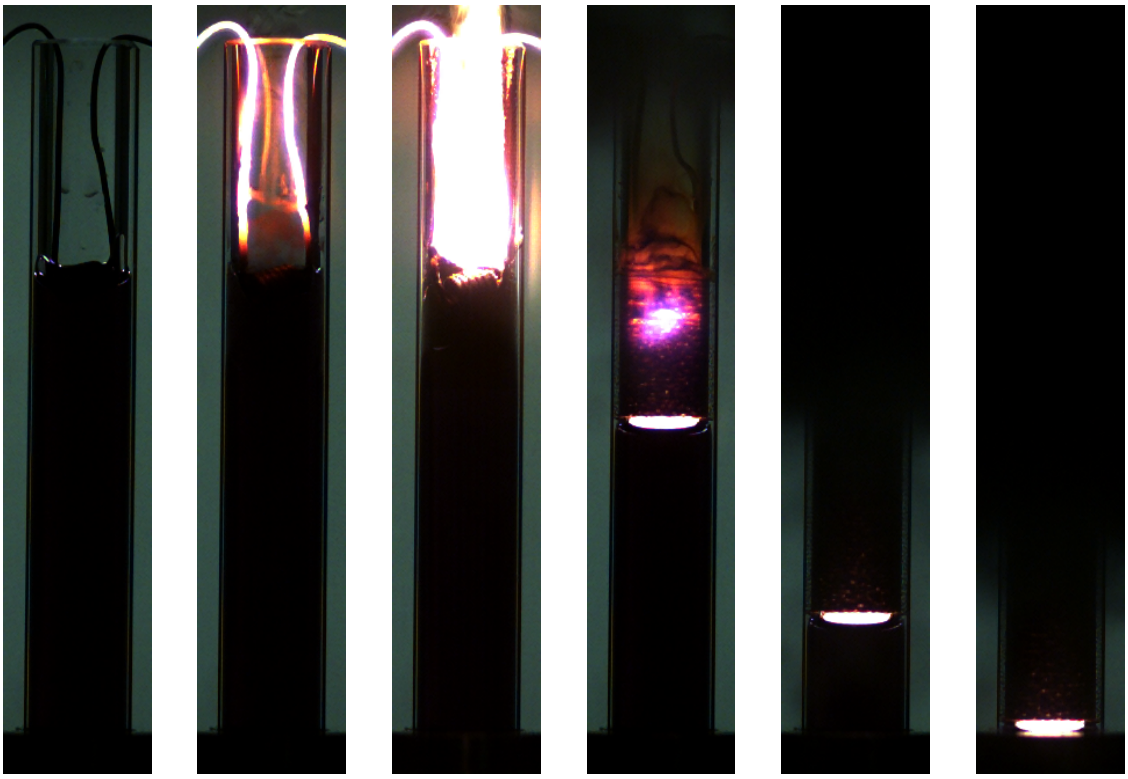

(a) T -0 s (b) T +2 s (c) T +6.1 s (d) T +12 s (e) T +22 s (f) T +27.5s

Figure 6.5: Frames from a CAA test at 5 MPa using the standard ignition method. (a) Power supply is turned on. (b) Wire reaches equilibrium temperature above 1000°C. (c) Ignition. (d)-(e) Stable combustion. (f) Flame reaches bottom of tube.

when comparing the combustion process at low pressures, CAA burned with a significantly less stable flame, unlike both OMC1 mixtures that when ignited, burned with a stable flame.

6.2.3 Inhibitors

The inhibitor additives OSC1 and BUT were, with one exception, tested only in combination with catalyst additives. For this reason these results will be discussed by first comparing the higher concentration OMC1 mixture with and without the addition of inhibitors. The same will then be done for the CAA propellant mixture.

The combustion rates of the mixtures containing OSC1 or BUT in combination with OMC1 in the higher concentration are plotted in figure 6.6. As reference the combustion rates for OMC1 without inhibitor additives and the previously used values for neat NM were added. Their addition resulted in an overall reduction of burning rates to a similar extent for both OSC1 and BUT, with the OSC1 mixture showing higher combustion rates at pressures below 3.5 MPa. The most notable effect, however, is that while BUT increases the minimum pressure at which combustion could be achieved to 2.02 MPa in comparison to the basic OMC1 mixture, as could be expected from an inhibitor, OSC1 further extends the pressure range to pressures as low as 1.24 MPa. This observation becomes even more notable when the combustion rate for the mixture containing only

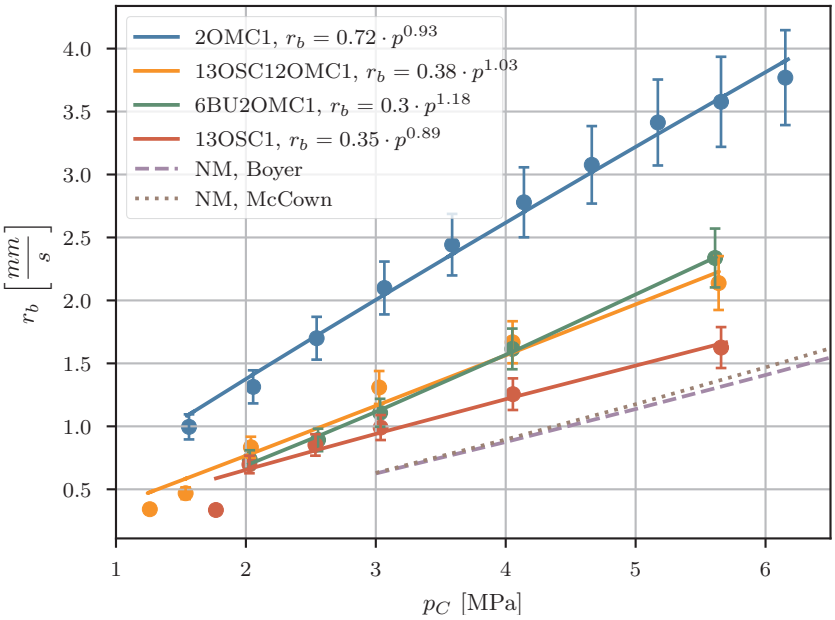

Figure 6.6: Combustion rates for mixtures of NM, OMC1 catalyst additive in its higher concentration and both inhibitor additives. For each pressure level at which tests were conducted the mean values for r_b and p were calculated. Error bars indicate the estimated error for the combustion rate measurements. As references the combustion rates of pure NM and two mixtures, one containing only the OMC1 catalyst and one containing only the OSC1 inhibitor, were added.

OSC1 is considered. It reaches a minimum combustion pressure of 1.77 MPa, which is above both the catalyst-inhibitor mixture (1.24 MPa) and the single catalyst mixture (1.54 MPa). Knowing this, it can be assumed that some interaction between the two additives takes place to lower the minimum pressure at which combustion is achievable. Furthermore, while not shown in this plot in order to maintain readability, the same effect was observed for the mixture containing the lower concentration of OMC1 in combination with OSC1 likewise at a lower concentration. For this a reduction of the minimum pressure from 1.74 MPa for the lower concentration OMC1 mixture to 1.53 MPa for the mixture containing both could be observed. When considering the regression analysis coefficients in 6.3 only a negligible difference between a and n of both the higher and lower concentration OMC1 and OSC1 mixtures is in evidence.

Figure 6.7 shows the combustion rates for the propellant mixtures containing both the CAA catalyst additive and the OSC1 inhibitor additive. A mixture containing BUT is not listed, since no sustained combustion could be achieved for this mixture (see table 6.2). The effect of OSC1 is not as pronounced for CAA mixtures as it was for those containing OMC1. A slight increase in combustion rates at pressures below 4.5 MPa can be observed. Furthermore, unlike the previously discussed case, the minimum pressure at which sustained combustion could be achieved remains unchanged even with the addition of OSC1.

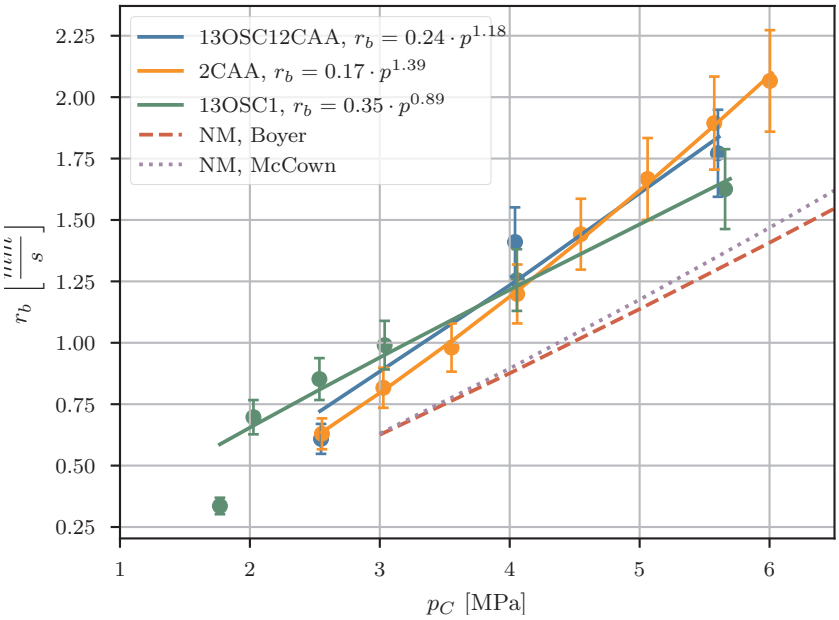

Figure 6.7: Combustion rates for mixtures of NM, the CAA catalyst additive and the OSC1 inhibitor additives. For each pressure level at which tests were conducted the mean values for r_b and p were calculated. Error bars indicate the estimated error for the combustion rate measurements. As references the combustion rates of neat NM and two mixtures, one containing only the CAA catalyst and one containing only the OSC1 inhibitor, were added.

OSC1, while considered an inhibitor, caused an overall increase in combustion rates when added to neat NM. The temperature coefficient a experienced a significant increase, while the pressure exponent was reduced to $n < 1$ making the curve regressive in nature. This effect can be seen again for the mixture of OSC1 and CAA. The temperature coefficient a experiences a slight increase while n is reduced, in turn reducing the pressure sensitivity when compared to the mixture containing only CAA. This leads to an increase in combustion rates at pressures below 4.5 MPa. In combination with OMC1 however, a different behavior was observed. As a is greater for these catalyst mixtures than for the inhibitor mixture, its addition causes a reduction in a. The pressure exponent on the other hand experiences a increase for both combinations, resulting in values $n > 1$ making both curves slightly progressive from previously being regressive without the addition of OSC1.

A mixture containing only BUT was not tested, therefore no observations on its effect the combustion behavior of neat NM can be made. In combination with OMC1 it caused a significant reduction of a and a equally significant increase in n increasing pressure sensitivity and, similar to OSC1's effect, making the curve progressive.

OSC1

In total 55 tests were done with various mixtures containing OSC1, 16 of these with a mixture containing only the inhibitor. The others were combinations of OSC1 with catalyst additives. Of those 16 tests 11 were successful. This propellant mixture proved difficult to ignite with all of the above mentioned failures resulting from ignition wires breaking before ignition could be achieved, though two of these tests were conducted below 1.77 MPa, which is the minimum pressure for sustained combustion determined for this mixture. Figures 6.8 and 6.9 show images from two tests conducted at 1.77 MPa and 5.5 MPa. The previously mentioned issues of exhaust gases obscuring the cameras view were more pronounced for this test series. The reason for this is that, in addition to the low combustion rates at low pressures, this mixture burned with significantly less intensity than the mixture containing catalyst additives. Additionally, a high ignition delay led to more vapor forming before the burning surface began to move downwards. These issues

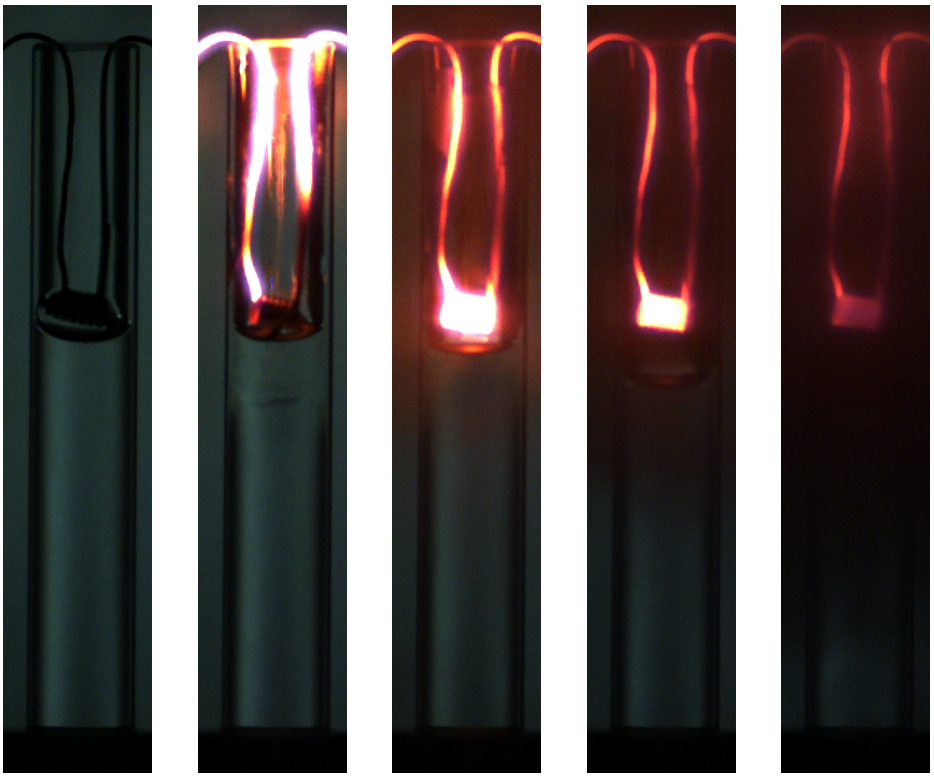

(a) T -0 s (b) T +6.5 s (c) T +18.5 s (d) T +25 s (e) T +33 s

Figure 6.8: Frames from a OSC1 test at 1.77 MPa using the standard ignition method. (a) Power supply is turned on. (b) Wire reaches equilibrium temperature above 1000°C. (c) Ignition. (d) Stable combustion. (e) Flame is obscured by exhaust gases. All of the propellant was burned, however.

can be seen in the low pressure test footage in figure 6.8. After the wire reaches its equilibrium temperature another 12 s pass before the propellant ignites. At T +25 s the flame is already barely visible in figure and at T +33 s it is completely blocked from view. An inspection after the test was completed showed that the tube was empty and all of the propellant had burned proving that, while it was not observable with the HS camera, sustained combustion was achieved at this

pressure. An evaluation of the footage produced at the lower end of the pressure range with the image analysis tool proved to be difficult, since only a small segment of each test runs footage was usable. At higher pressures this issue was still present, but to a lesser extent as shown by the images in figure 6.9. To improve visibility of the flame, shutter speeds were increased compared

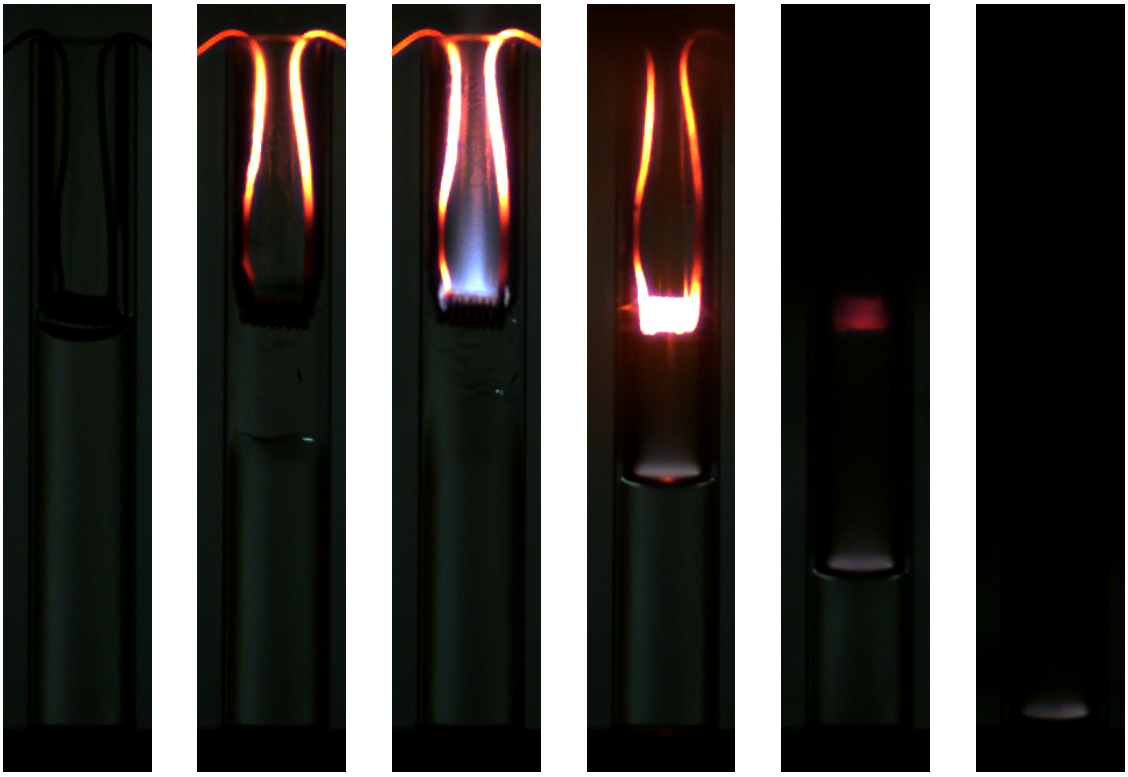

(a) T -0 s (b) T +8 s (c) T +10.6 s (d) T +17 s (e) T +22 s (f) T +30 s

Figure 6.9: Frames from a OSC1 test at 5.5 MPa using the standard ignition method. (a) Power supply is turned on. (b) Wire reaches equilibrium temperature above 1000°C. (c) Ignition. (d)-(e) Stable combustion. (f) Flame reaches bottom of tube.

to earlier tests, in turn making the frame at T -0 s barely visible. Compared the catalyst additive tests however, flame visibility was still low. Starting from T +22 s the flame remains barely visible until it reaches the bottom of the tube.

n-Butanol

BUT was tested 16 times but only in combination with catalyst additives. Of these tests 12 were conducted for a mixture containing OMC1 in its higher concentration of which 10 were successful. Both failed tests were conducted to verify the minimum combustion pressure. The remaining four tests, which involved mixtures containing CAA in addition to the inhibitor, were all unsuccessful. Attempts were made at pressures up to 5.5 MPa and while the propellant did ignite, no sustainable combustion was achieved and the flame extinguished itself shortly after the wire broke and the current was interrupted. It was therefore concluded that, similar to the neat NM tests, combustion was not possible with the setup used in this work.

6.2.4 Discussion of Results

Table 6.3 shows an overview of the calculated coefficients for each propellant mixture, where a is the temperature coefficient and n the pressure exponent. With an increase in combustion rate

Table 6.3: Temperature coefficient a and pressure exponent n of the empirical power law function of the combustion rate r_b for each propellant mixture. Calculated using a regression analysis with the results of the strand burner tests.

Mixture	**a**	**n**	**range [MPa]**
neat NM [7]	0.173	1.17	$3<p<15$
neat NM [8]	0.165	1.22	$3<p<13$
2OMC1	0.724	0.93	$1.54<p<6.17$
1OMC1	0.544	0.96	$1.74<p<5.83$
2CAA	0.172	1.39	$2.55<p<6.02$
13OSC1	0.352	0.89	$1.77<p<5.7$
13OSC12OMC1	0.375	1.03	$1.24<p<5.64$
13OSC12CAA	0.240	1.18	$2.54<p<5.61$
10OSC11OMC1	0.381	1.01	$1.53<p<5.6$
6BUT2OMC1	0.303	1.18	$2.02<p<5.62$
6BUT2CAA	-	-	-

of 219% at 3 MPa the 2 wt.% OMC1 produced the the best results regarding combustion rate, significantly outperforming the mixture containing CAA. Additionally a lowering of the minimum pressure at which sustained combustion can be achieved from 3 MPa (neat NM) to 1.54 MPa was observed. The the addition of 13 wt.% OSC1, despite it being selected for its inhibiting properties, also burned with an increased combustion rate (47% increase at 3 MPa). Most notably however the mixture containing 13 wt.% OSC1 and 2 wt.% OMC1 burned at even lower pressures (1.24 MPa) while still achieving a 84% increase in combustion rate at 3 MPa.

6.3 Image Analysis

As no results could be generated for neat NM in the run-in test campaign, the results of the image analysis tool could not be verified through comparison with results from previous studies. However, the results generated for the additive mixtures were highly repeatable, indicating the presence of systematic errors, though it is not possible to quantify these errors. While no comparison with results from other studies can be made, a systemic error would nevertheless allow a comparison of the results generated with the setup developed as part of this thesis among each other. Therefore it is possible and valid to draw conclusions regarding the effect the tested additives on neat NM combustion.
In the following sections the two main functions of the image analysis tool are reviewed.

6.3.1 Flame Position Tracking

As mentioned in section 6.2 the main issue encountered during evaluation of the HS-camera footage was connected to bad visibility due to exhaust gases and vapors obstructing the view of the camera. As a result a high amount of manual calibration was needed. This process was simplified by the calibration script implemented for this purpose. It enabled quick and easy adjustment of the threshold values in order to obtain good results. Apart from the view obstruction, switching to different propellant mixtures also required re-calibration of the threshold values. The reason for this was that different mixtures burned at different light intensities requiring adjustment of the HS-camera recording settings (shutter speed), which led to an overall change in brightness of the footage, with darker footage making it generally easier to identify and select the correct edges. Additionally, the varying cleanliness of the combustion between the propellant mixtures also influenced flame position tracking process. In the case of mixtures containing OMC1 the soot formed during a test run would settle on the inner walls of the glass tube, so that only the burning surface was visible in most cases, which made selection of the correct edge during flame position tracking simpler. In the case of neat NM on the other hand, combustion produced no soot and shutter speed was lower resulting in brighter images. This footage required a comparatively high amount of manual calibration as reflections on the tube edges and the broken ignition wire would make selection of the correct edge more difficult. Additionally, threshold values would require readjustment even for other neat NM tests conducted with the same camera settings due to the widely varying quality of the footage.

6.3.2 Scale Determination

Figure 6.10 shows two plots from the higher concentration OMC1 test series. The top plot is the combustion rate regression analysis including all datapoints and the bottom one is the same analysis done with the slope initially determined during the image analysis process before the values were converted from pixels to mm. The comparison of these plots shows how the mm/pixel-scale effects the final values for the combustion rate. While in general there is only slight variation between the datapoints in both plots, meaning that for the majority of test runs the mm/pixel-scale has similar values, in some cases the value differs significantly. One such case has been highlighted with a red circle in the combustion rate plot. For this test run the scale determined during image analysis does not match the values determined for the other test runs.

However, as this was the only occurrence of such a discrepancy during all of the testing conducted in the course of this work, it can be assumed that the measurements are highly repeatable.

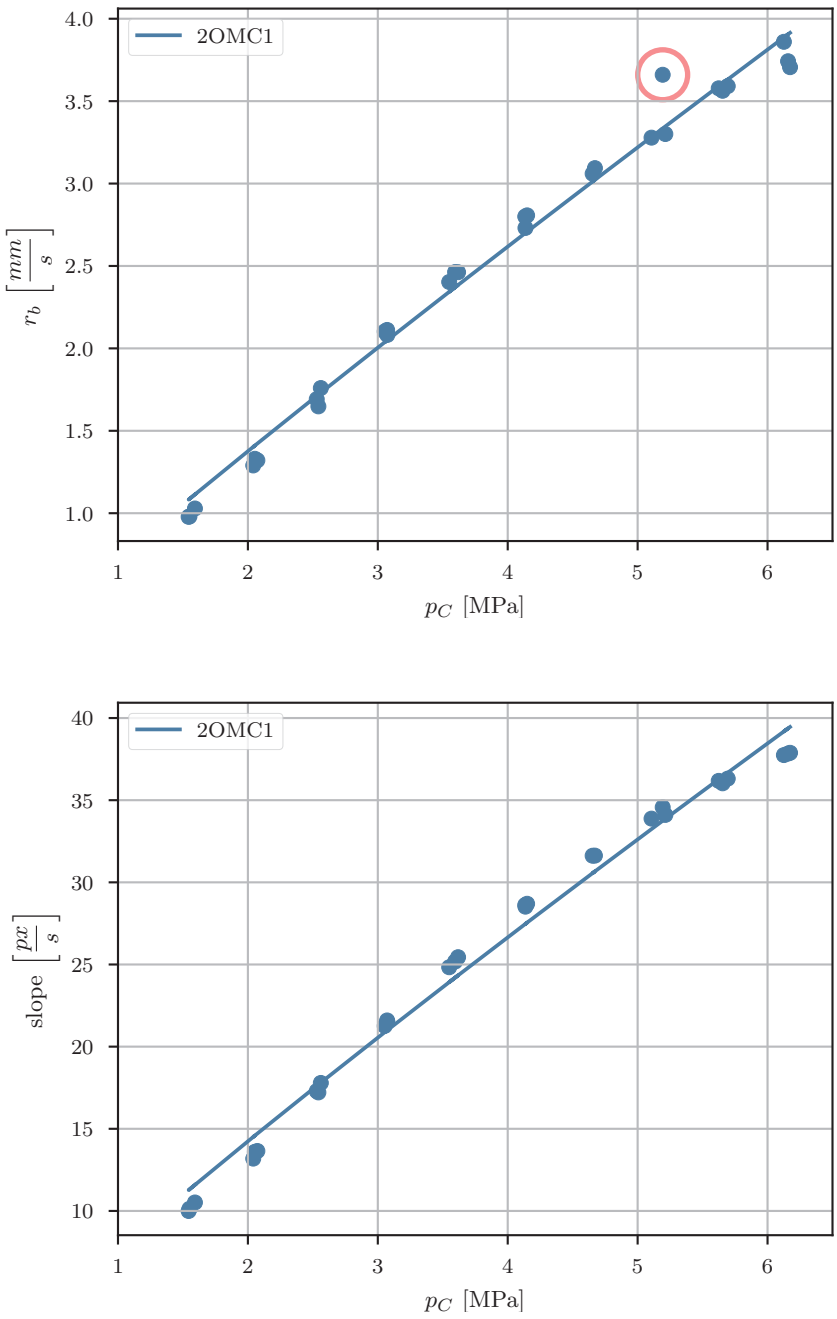

Figure 6.10: Comparison of combustion rate r_b and slope regression analyses. Circled datapoint (red) demonstrates error caused by deviation in scale between tests of the same series.

7 Conclusion

In the following chapter the experimental setup and image analysis tool that were developed are reviewed. Additionally, key findings of the combustion rate studies conducted within this work are presented.

7.1 Experimental Setup

The experimental setup that was developed as part of this thesis is a liquid propellant strand burner which enables the study of liquid monopropellant combustion rates. The baseline of the design is a combustion chamber, that was developed in the past at the German Aerospace Center, and is equipped with opposed viewing windows, allowing optical observation of the combustion process within. Similar strand burner test stands developed for previous studies were reviewed in order to determine the most suitable solutions for key components and features such as the method of ignition, pressure regulation and methods of measuring the combustion rate. For the latter feature, a high-speed camera was chosen to record the combustion process and allow subsequent analysis of the footage using an image analysis tool that was implemented for this purpose. The ignition system was designed in such a way that many of the methods identified in the literature review could be implemented and tested. A control and data acquisition system was developed that uses a programmable logic controller unit based on a Raspberry Pi single-board computer connected to a microcontroller. This system enables a fully remote and therefore safe operation of the valves, ignition system and HS camera via a custom graphical user interface. The proper functioning of the experimental setup was demonstrated in two separate test campaigns in which a total of 164 tests were conducted.

A review of the final design showed that the requirements defined as part of the design process were mostly met. Two requirements were only partially met. The first (F.4) defined that the setup shall enable combustion rate measurements. This was only partially fulfilled, as it was not possible to verify the results via comparison with results from other studies. The reason for this is that it was not possible to generate results in the initial run-in test campaign which was originally intended to supply a baseline for subsequent test campaigns. The second requirement (D.1) was also only partially fulfilled. It stated that the ignition system shall be characterized with a well-defined ignition temperature or energy. This system utilized a resistance heating wire made of nichrome to ignite the propellant. Multiple methods to actively measure the wire temperature were unsuccessful. As a less accurate yet valid solution it was decided to rely upon to wire temperature data provided by the manufacturer and to visually observe the power supply output to estimate the ignition temperature.

In summary the developed strand burner test stand fulfilled most of the defined requirements and proved adequate for the purpose of this study. Modifications which would have been necessary to fully accommodate all requirements would have resulted in significant cost increases.

7.2 Image Analysis Tool

A custom image analysis tool was implemented in Python using the OpenCV software library in order to evaluate the recorded HS camera footage and determine combustion rates. The analysis is performed in two steps that are executed in parallel. The first step is to track flame position while iterating over the separate frames and compile flame position history data. These data are then used to determine at which rate the flame moves downwards through the tube. Since this value is measured in pixels the next step is to determine the mm/pixel-scale with which the combustion rate in mm can be calculated. Calibration scripts were implemented for both processing steps in order to easily adjust the image processing settings to adapt to variations in image quality between different propellant mixtures and their visual combustion characteristics. While the results could not be verified they were highly repeatable, allowing the study of the effects of the tested additives by comparison among each other viable.

7.3 Combustion Rate Studies

During the additives test campaign two catalyst (OMC1 and CAA) and two inhibitor (OSC1 and BUT) additives were tested. Both catalyst additives performed as expected, increasing overall combustion rates when compared to neat NM, improving ignitability at low pressures and lowering the minimum pressure at which sustained combustion could be achieved. Of the two catalyst additives the iron-based organometallic compound (OMC1) produced the best results, significantly outperforming the mixture containing CAA. The addition of inhibitors to the mixtures containing catalyst additives resulted in a reduction of overall combustion rates, as was to be expected. While in the case of BUT, this was the only effect observed, the addition of OSC1 resulted in a further decrease of minimum pressures when combined with the OMC1 catalyst additive. With a minimum pressure of 1.24 MPa the mixture containing a higher concentration of OMC1 performed at a pressure level comparable to current SOTA hydrazine thrusters. This combination of catalyst and inhibitor additive therefore holds great promise as a green monopropellant alternative to hydrazine.

During the run-in test campaign, sustained combustion of neat nitromethane could not be achieved with the ignition method selected within this work. Therefore, no verification of the results through comparison with results from previous studies was possible. However, the results generated in the following test campaign were observed to be highly repeatable making comparison of those results among each other, in order to study the effect of the additives, valid and reasonable. While initially no sustained combustion could be achieved, slight adjustments to the selected ignition method, which could be easily implemented due to the flexibility inherent in the developed setup regarding the ignition method, resulted in other findings worth mentioning. Positioning the wire coil close

to the bottom of the tube, such that the majority of the propellant column was above the coil, resulted in successful ignition and sustained combustion. In comparison to results generated in previous studies, the combustion rates measured in these tests were significantly higher, indicating that the changes in the ignition method had an effect. The assumption was made that this could either be a result of the preheating that occurred prior to ignition or that the wire material (NiCr) may have some catalytic effect on NM combustion. However, as this method of ignition can not be considered representative for the use of NM as a monopropellant, as was the objective of the present work, these tests were considered unsuccessful and neat NM tests were abandoned.

8 Future Work

In the following chapter some suggestions for future work regarding the experimental setup, the image analysis tool and NM combustion rate studies are presented.

8.1 Experimental Setup

A major issue encountered during testing was the obstruction of vision due to exhaust gases and vapors. When this occurred, generally at lower pressures and subsequently lower combustion rates, image quality suffered to an extent that made the processing of the recorded footage significantly more difficult and less robust. This footage required considerable of manual calibration in order to produce acceptable results. Therefore, implementing a system to remove exhaust gases from the combustion chamber during a test run would greatly improve the functionality of the strand burner test stand.

Another point of improvement is connected to the manner in which the HS camera is positioned in front of the combustion chamber. Since it was placed in front of the fume hood on top of a table great care needed to be taken in order to ensure that its positioning and orientation were not changed. However, instances did occur where the table or the camera was nudged during test preparation or turn around, which required readjustment. A redesign of the setup, whereby the camera mount is integrated into the structure carrying the combustion chamber would solve this issue. Additionally, this would allow a precise calibration of the camera using calibration patterns (i.e. checkerboards), which would render the step of scale determination during the image analysis process unnecessary.

The final point of improvement is meant to address the issues encountered during characterization of the ignition method. The requirement regarding this issue demanded a well defined ignition temperature. A direct measurement of wire temperature could not be realized in the course of this work and the wire manufacturer's data was used instead. While this method is reasonable, it relied on visual observation of the power supply output and manually noting the readings on the power supply's display. This could be improved upon by implementing a system to read and store the power supply output automatically, ideally integrated into the data acquisition and control system. Improving the characterization of the ignition method would allow more valid observations regarding characteristics (i.e. ignitability, ignition delay) of the tested propellants.

8.2 Image Analysis

With the proposed changes to the experimental setup, image quality could be better controlled and predicted, potentially enabling increased automation of the image analysis process. In its

current state, separate test runs, even with the same propellant, require separate analysis. If it could be relied upon that image quality and camera positioning are identical between each test this would no longer be necessary and the entire footage of, for example, one day of testing could be processed without further manual input.
Another avenue worth exploring, with the goal to improve image quality, would be to tackle this issue through common HS imaging and computer vision approaches and practices. In order to complete the work in this thesis in the time given and quickly generate results, little effort was made to optimize camera settings apart from adjustments made to the shutter speed. The viewing software provided by the camera manufacturer offers a multitude of tools that, when used correctly, have the potential to greatly improve image quality, such as auto-focus capabilities (focus assistant) and Dual Slope Shutter to prevent over exposure without post processing. Correct lighting also plays a significant role in HS imaging and could improve image quality.

8.3 Combustion Rate Studies

The main issue encountered during the combustion rate studies was the inability to initiate sustained combustion of neat NM. According to previous neat NM combustion rate studies conducted with similar liquid propellant strand burner test stands, ignition and sustained combustion of the propellant should have been possible at the pressures that this was attempted in the run-in test campaign. However, these sources only reported difficulties igniting the propellant and no inability to achieve sustained combustion. In future work this issue could be further addressed by attempting ignition using solid booster pellets. This was the common solution for addressing ignition issues found when reviewing past studies, but was decided against in this work to retain simplicity in the setup and because other sources suggested that it is possible to ignite the propellant without the aid of a solid booster.

In an attempt to address this issue without the aid of a solid booster, the ignition method used in this work was adjusted. This lead to new findings that suggested that the resistance heating wire material NiCr could have a catalytic effect on NM combustion, where a significant increase in combustion rate in comparison to values reported in other studies was observed. Further investigation regarding these results could be interesting as initiating the chemical decomposition reaction of monopropellants using catalytic materials is the preferred choice for monopropellant thrusters. An alternative explanation for this effect was also proposed in this work. The adjusted ignition method was named the ‘preheater’ method since the ignition wire acted similar to a submersible/immersion heater and preheated the propellant prior to ignition. Determining the explanation for the observed effect could be an interesting topic to explore in the future.

Finally, the proposed modifications to the ignition system mentioned above would allow the study of the effects different pressures and additives have on the ignitability and ignition delay of nitromethane.

Bibliography

[1] C. D. Brown, *Spacecraft propulsion*. American Institute of Aeronautics and Astronautics, 1996.

[2] NASA, "Space shuttle forward reaction control thrusters," Aug. 2005, "Last accessed 23 April 2022". [Online]. Available: http://spaceflight.nasa.gov/gallery/images/shuttle/sts-114/html/s114e6215.html

[3] S. Li, H. Yan, Z. Wang, Y. Tang, Z. Yao, and S. Li, "Catalytic decomposition and burning of a dual-mode ionic liquid propellant," *Energy & Fuels*, vol. 35, no. 22, pp. 18 716–18 725, nov 2021.

[4] W. M. Marshall and M. C. Deans, "Recommended figures of merit for green monopropellants," in *49th AIAA/ASME/SAE/ASEE Joint Propulsion Conference*. American Institute of Aeronautics and Astronautics, jul 2013.

[5] A. Mayer and W. Wieling, "Green propulsion research at TNO the netherlands," *Transactions on Aerospace Research*, vol. 2018, no. 4, pp. 1–24, dec 2018.

[6] European Space Agency, "Webb fuelled for launch," Dec. 2021, "Last accessed 22 September 2022". [Online]. Available: https://www.esa.int/ESA_Multimedia/Images/2021/12/Webb_fuelled_for_launch

[7] E. Boyer and K. Kuo, "Characteristics of nitromethane for propulsion applications," in *44th AIAA Aerospace Sciences Meeting and Exhibit*. American Institute of Aeronautics and Astronautics, jan 2006.

[8] K. W. McCown, A. R. Demko, and E. L. Petersen, "Experimental techniques to study linear burning rates of heterogeneous liquid monopropellants," *Journal of Propulsion and Power*, vol. 30, no. 4, pp. 1027–1037, jul 2014.

[9] European Chemicals Agency, "Nitromethane substance infocard," "Last accessed 26 September 2022". [Online]. Available: https://echa.europa.eu/de/substance-information/-/substanceinfo/100.000.797

[10] M. Kurilov, L. Werling, M. Negri, C. Kirchberger, and S. Schlechtriem, "Impact sensitiveness of nitromethane-based green-propellant precursor mixtures," in *Space Propulsion Conference, Estoril, Portugal*. German Aerospace Center, May 2022.

[11] G. P. Sutton, *Rocket propulsion elements*. Wiley, 2010.

[12] H. M. Kindsvater, K. K. Kendall, K. H. Mueller, and P. P. Datner, "Research on nitromethane," Aerojet Engineering Cooperation, Tech. Rep., 1951.

[13] J. E. Boyer, "Combustion characteristics and flame strucuture of nitromethane liquid monopropellant," Ph.D. dissertation, Pennsylvania State University, Dec. 2005.

[14] G. Derk, "High-pressure burning-rates of ja2 and nitromethane porpellants," Ph.D. dissertation, Pennsylvania State Univsersity, 2019.

[15] K. W. McCown and E. L. Petersen, "Effects of nano-scale additives on the linear burning rate of nitromethane," *Combustion and Flame*, vol. 161, no. 7, pp. 1935–1943, jul 2014.

[16] J. Sabourin, R. Yetter, B. Asay, J. Lloyd, V. Sanders, G. Risha, and S. Son, "Effect of nano-aluminum and fumed silica particles on deflagration and detonation of nitromethane," *Propellants, Explosives, Pyrotechnics*, vol. 34, no. 5, pp. 385–393, oct 2009.

[17] J. L. Sabourin, R. A. Yetter, and V. S. Parimi, "Exploring the effects of nanostructured particles on liquid nitromethane combustion," *Journal of Propulsion and Power*, vol. 26, no. 5, pp. 1006–1015, sep 2010.

[18] J. L. Sabourin, D. M. Dabbs, R. A. Yetter, F. L. Dryer, and I. A. Aksay, "Functionalized graphene sheet colloids for enhanced fuel/propellant combustion," *ACS Nano*, vol. 3, no. 12, pp. 3945–3954, nov 2009.

[19] J. Clark, *Ignition! An Informal History of Liquid Rocket Propellants.* Rutgers University Press Classics, 2018.

[20] M. J. L. Turner, *Rocket and Spacecraft Propulsion Principles, Practice and New Developments.* Springer Berlin Heidelberg, 2009.

[21] O. Bozic, *Space Propulsion Lecture Script.* Institute of Space Systems, TU Braunschweig, 2018.

[22] D. K. Huzel and D. H. Huang, *Modern Engineering for Design of Liquid-Propellant Rocket Engines (Progress in Astronautics and Aeronautics).* AIAA (American Institute of Aeronautics and Astronautics, 1992.

[23] Surrey Satellite Technology Ltd (SSTL), "Sstl awarded innovate uk grant for propulsion system," 2016, "Last accessed 02 October 2022". [Online]. Available: https://www.sstl.co.uk/media-hub/latest-news/2016/sstl-awarded-innovate-uk-grant-for-propulsion-system

[24] R. L. Sackheim and R. K. Masse, "Green propulsion advancement: Challenging the maturity of monopropellant hydrazine," *Journal of Propulsion and Power*, vol. 30, no. 2, pp. 265–276, mar 2014.

[25] A. E. S. Nosseir, A. Cervone, and A. Pasini, "Review of state-of-the-art green monopropellants: For propulsion systems analysts and designers," *Aerospace*, vol. 8, no. 1, p. 20, jan 2021.

[26] O. Morgan and D. Meinhardt, "Monopropellant selection criteria - hydrazine and other options," in *35th Joint Propulsion Conference and Exhibit.* American Institute of Aeronautics and Astronautics, jun 1999.

[27] L. Ziemer, “Influence of organometallic complexesand carbon nanoparticles onnitromethane droplet combustion,” Master’s thesis, Institute of Space Systems and DLR Institute of Space Propulsion, Nov. 2021.

[28] P. Linstrom, “Nist chemistry webbook, nist standard reference database 69,” 1997.

[29] European Cooperation for Space Standardization, “Space engineering - technical requirements specification,” ESA Requirements and Standards Division, techreport, Mar. 2009, eCSS-E-ST-10-06C, 6 March 2009.

[30] *Realization and Run-In of a Gel Combustion Chamber with Optical Access.* Proceedings of the 7th European Conference for Aeronautics and Space Sciences. Milano, Italy, 3-6 july 2017, 2017.

[31] M. M. Gudnason, “Characterization of potassiumnitrate - sugar alcohol basedsolid rocket propellants,” Master’s thesis, Technical University of Denmark, Department of Chemistry, 2010.

[32] G. Risha, S. Son, R. Yetter, V. Yang, and B. Tappan, “Combustion of nano-aluminum and liquid water,” *Proceedings of the Combustion Institute*, vol. 31, no. 2, pp. 2029–2036, jan 2007.

[33] B. J. McBride and S. Gordon, “Computer program for caclulation of complex chemical equilibrium compositions and applications: I. analysis,” National Aeronautics and Space Administration, Tech. Rep., 1994, nASA Reference Publication 1311.

[34] A. Schmidt, *Technical Thermodynamics for Engineers.* Springer International Publishing, 2019.

[35] WIKA Alexander Wiegand SE & Co. KG, “Data Sheet: Pressure transmitter for general industrial applications Model A-10,” 2022, "Last accessed 22 September 2022". [Online]. Available: https://www.wika.com/en-en/a_10.WIKA

[36] C. C. Fuller, J. B. Sinrud, R. A. Schwind, M. S. Klassen, C. F. Goldsmith, and R. A. Walker, “A continuous flow liquid propellant strand burner for high pressure monopropellant and bipropellant combustion studies,” *Review of Scientific Instruments*, vol. 92, no. 2, p. 025106, feb 2021.

[37] Y.-P. Chang, E. Boyer, and K. K. Kuo, “Combustion behavior and flame structure of XM46 liquid propellant,” *Journal of Propulsion and Power*, vol. 17, no. 4, pp. 800–808, jul 2001.

[38] G. Dyos, *Handbook of Electrical Resistivity.* Institution of Engineering & Technology, 2012.

[39] D. C. Giancoli, *Physics.* Prentice Hall, 2004.

[40] Omega Engineering, Inc., “Data Sheet: Resistance Heating Wire Nickel-Chromium Alloy 80% Nickel 20% Chromium,” 2022, "Last accessed 22 September 2022". [Online]. Available: https://www.omega.com/en-us/accessories/electrical-components/heating-wire-and-cables/p/NI80

[41] T. Katsumi, H. Kodama, T. Matsuo, H. Ogawa, N. Tsuboi, and K. Hori, "Combustion characteristics of a hydroxylammonium nitrate based liquid propellant. combustion mechanism and application to thrusters," *Combustion, Explosion, and Shock Waves*, vol. 45, no. 4, pp. 442–453, jul 2009.

[42] M. A. Phillips, "Development of an optically accessible high-pressure strand burner and the experimental determination of the burn rate of high temperature thermally degraded htpb/ap/al solid propellant combustion," Master's thesis, Auburn University, 2020.

[43] V. A. Arkhipov, S. S. Bondarchuk, and A. G. Korotkikh, "Comparative analysis of methods for measuring the transient burning rate. i. research methods," *Combustion, Explosion, and Shock Waves*, vol. 46, no. 5, pp. 564–569, sep 2010.

[44] Y. Ide, T. Takahashi, K. Iwai, K. Nozoe, H. Habu, and S. Tokudome, "Combustion characteristics of an ammonium-dinitramide-based ionic liquid propellant," *Transactions of the Japan Society for Aeronautical and Space Sciences, Aerospace Technology Japan*, vol. 14, no. ists30, pp. Pa_89–Pa_94, 2016.

[45] Carl Roth Gmbh & Co. Kg, "Nitromethane 98,5 %, for synthesis," 2022, "Last accessed 26 September 2022". [Online]. Available: https://www.carlroth.com/com/en/aliphatic-building-blocks/nitromethane/p/4406.1

[46] OpenCV team, "Opencv python documentation," 2022, "Last accessed 22 September 2022". [Online]. Available: https://docs.opencv.org/

List of Figures

List of Tables

List of Symbols